



UNIVERSIDAD TECNICA  
FEDERICO SANTA MARIA

Departamento de Obras Civiles

## **WIND-EFFECTS ON BAR-BUILT ESTUARY HYDRODYNAMICS**

Memoria de Título presentada por

**Dhannai Tamara Sepúlveda González**

como requisito parcial para optar al título de la carrera de

**Ingeniería Civil**

y el grado de

**Magíster en Ciencias de la Ingeniería Civil**

Profesor Guía  
Megan Elizabeth Williams

SEPTEMBER, 2023



UNIVERSIDAD TECNICA  
FEDERICO SANTA MARIA

TÍTULO DE LA TESIS:

**WIND-EFFECTS ON A BAR-BUILT ESTUARY HYDRODYNAMICS**

AUTOR:

**DHANNAI TAMARA SEPÚLVEDA GONZÁLEZ**

TRABAJO DE MEMORIA, presentado como requisito parcial para optar al grado de MAGÍSTER EN CIENCIAS DE LA INGENIERIA CIVIL de la Universidad Técnica Federico Santa María.

Nombre Profesor Guía: Megan Williams

Nombre Miembro 1 Comisión: .....

Nombre Miembro 2 Comisión: .....

Valparaíso, Chile, Septiembre, 2023

# WIND-EFFECTS ON BAR-BUILT ESTUARY HYDRODYNAMICS

Dhannai Sepúlveda<sup>1</sup>, Megan Williams<sup>1</sup>

1 Universidad Técnica Federico Santa María

## Abstract

Although bar-built estuaries are widespread on Mediterranean coasts all around the world, including central Chile, little research has been undertaken on its closed state, when its system is transformed into a salty lagoon. Understanding the dependence of hydrodynamic response and thermohaline-stratification on strong wind events and its associated transport and mixing is of prime importance on the impact of water quality and eutrophication on ecosystems in coastal lagoons. In this study, we analyze the role of external factors such as wind velocities, freshwater flow, and wave overtopping in the hydrodynamics of a shallow, highly salt-stratified bar-built estuary. Vertical mixing and forcing currents, governed by wind surface stress, were quantified for diurnal and hourly time scales.

Data collected in early 2012 at Pescadero Estuary, California shows that in a close state there is a strong stratification and strong wind events during its closed state and due to its morphology wind is channelized into the along-estuary direction, causing the lagoon to receive mainly local forcing. Frequency spectral analysis is used to identify seiches on the surface due to upwelling caused by the wind. Wavelet analysis was also used to identify wave overtopping on the sand bar and observe the real effect of saline water entering the estuary. During strong wind events, buoyancy frequency was reduced to almost 0 from the  $0.1 \text{ s}^{-2}$  that the estuary usually had, and in some cases not return to its original value, showing upwelling and mixing of the water column. However, these effects varied over time depending on water level due to constant inflow from Pescadero and Butano creek. Some indicators like potential anomaly showed a good correlation with wind stress during the studied period. These preliminary findings show that wind effects are dominant in forcing vertical exchange of layers and generating currents at Pescadero.

*Key words:* *bar-built estuaries, wind stress, stratification, upwelling, mixing*

## **ACKNOWLEDGEMENTS (AGRADECIMIENTOS)**

El buen término de este magíster se debe principalmente al apoyo económico de la Universidad Técnica Federico Santa María con su beca de arancel que cubrió completamente mis años de estudio en este programa y también al financiamiento entregado por ANID Fondecyt 11191077.

Quiero comenzar mis agradecimientos con las personas más importantes en mis años de estudios. A mi abuelita Georgina por siempre motivarme a dar lo mejor de mí y porque sin ella no estaría donde estoy, a mi mamá Sandra por ser mi apoyo emocional más fuerte y entregarme siempre su cariño, y a mi papá David por todos sus consejos de vida y por siempre contagiarde su alegría, quienes siempre estuvieron presentes en todo ámbito apoyándome con mi carrera y con mis proyectos personales. A mis amigas del alma que estuvieron presentes para los buenos y los malos momentos, con las que reí y lloré Karla y Francesca. A las amigas en las que siempre puedo confiar incondicionalmente y quienes siempre me van a escuchar y aconsejar, Daniela, Valentina, Ismaela y Paulina.

Agradecer igualmente a las personas que conocí en mi paso por la universidad partiendo por la profesora Megan, a quien agradezco por tomarme como estudiante, por todo lo que me enseñó en mis más de 2 años de Magíster y quien siempre me tuvo paciencia en lo que no entendía. A mis compañeros del equipo de Mecánica de Fluidos Ambiental con quienes tuvimos varias salidas a terreno y donde aprendí mucho. A quienes se volvieron como mi familia en los años de carrera, Claudio, Francisco y Mikel con quienes viví incontables aventuras en la época universitaria y en quienes siempre encontré apoyo en los momentos difíciles. Finalmente, agradecer a la persona que me ha acompañado por 7 años, aconsejandome, contagiándose su alegría y con quien las tardes y noches estudiando se volvieron más amenas. Gracias Bastian por apoyarme con mis metas y por ayudarme a ser la persona que soy hoy en día.

# Contents

<b>1</b>	<b>Introduction</b>	<b>7</b>
1.1	The Pescadero estuary . . . . .	8
1.2	Motivation . . . . .	9
<b>2</b>	<b>Objectives</b>	<b>9</b>
2.1	General objective . . . . .	9
2.2	Specific objectives . . . . .	10
<b>3</b>	<b>Literature review</b>	<b>10</b>
3.1	Bar-built estuaries in the ecosystem and the community . . . . .	10
3.2	How bar-built estuaries are studied in Chile and around the world . . . . .	11
3.3	Hydrodynamics of a stratified waterbody . . . . .	12
3.4	Pescadero estuary studies . . . . .	13
<b>4</b>	<b>Methods</b>	<b>14</b>
4.1	Field measurements . . . . .	14
4.2	External data . . . . .	15
4.3	Data processing . . . . .	16
4.3.1	Salinity and temperature . . . . .	16
4.3.2	Water velocity . . . . .	17
4.3.3	Wind velocity . . . . .	18
4.4	Analysis techniques . . . . .	19
4.4.1	Stratification . . . . .	19
4.4.2	Wind stress . . . . .	20
4.4.3	Surface fluctuations analysis . . . . .	21
<b>5</b>	<b>Results</b>	<b>21</b>
5.1	Conditions observed during the closed state . . . . .	22
5.1.1	Wind in the estuary . . . . .	22
5.1.2	Evolution of density structure . . . . .	24
5.1.3	Tidal and waves conditions . . . . .	25
5.1.4	Pescadero creek discharge . . . . .	27
5.1.5	Currents speed and direction . . . . .	27
5.1.6	Surface fluctuations . . . . .	27
5.2	Hydrodynamic controllers . . . . .	27
5.2.1	Stratification controllers . . . . .	28
5.2.2	Surface fluctuations controllers . . . . .	29
5.3	Wind-driven effects . . . . .	29
<b>6</b>	<b>Discussion</b>	<b>38</b>
6.1	Estuarine structure and morphology . . . . .	38
6.2	Analysis methods . . . . .	39
6.3	Wind stress mixing . . . . .	40
6.4	Wind-driven circulation . . . . .	41
6.5	Freshwater input . . . . .	44
6.6	Wave overtopping . . . . .	45

## List of Figures

1	Location of Pescadero Estuary on California's Coastline. Images reprocessed from Google Earth. . . . .	8
2	Pescadero estuary map and location of the moorings (NM: Near Mouth, ML: Mid-Lagoon, DC: Deep Channel and, PC: Pescadero Creek), meteorological station. Profile locations for CTD measurements in Fig. 2 are indicated by small "x". Diagram of the elevation view of Pescadero in the along-estuary direction with the locations of the sensors in the water column. . . . .	15
3	Time-series of instruments depth in all locations. The windowed data is the used in this study. . . . .	15
4	Anemometer for wind measurements. Model #05106, RM Young. (Williams, 2014) . . . . .	16
5	Stations and sites locations of the external data obtained for this study. . . . .	17
6	Timeseries of velocity data plotted in North and East directions in the water column. . . . .	18
7	Velocity data plotted in North-East and $u - v$ coordinates, and a map of Pescadero signaling the coordinates. . . . .	18
8	Time-series of wind velocity magnitude and direction. Wind velocity in North-East coordinates over the Pescadero map and in (u,v) coordinates. . . . .	19
9	Time-series of 0.3 times the total depth of the estuary at the location DC. . . . .	20
10	Step 1: Raw frequency spectral analysis. Step 2: Frequency spectral analysis with a noise reduction. Step 3: Frequency spectral analysis with a noise reduction and a detrend applied. Step 4: The obtained signal from step 3 is multiplied by a quadratic window shown in Eq. 9. . . . .	21
11	Time-series windowing the closed state of colormap of density in DC location in the water column height, where the black line represents the water level; wind speed in $u$ and $v$ direction. . . . .	22
12	Time-series of wind speed in $u$ and $v$ direction. . . . .	23
13	Windrose of the data collected in Pescadero from 15 Jan. to 20 Mar. Maximun speed registered in the studied period was 13.02 m/s . . . . .	23
14	Time-series windowing at both closure phases of temperature and salinity in NM, where 1 is the deepest sensor and 4 the shallowest, colormap of density in NM in the water column, where the black line represents the water level, and the change of the water level in a 10-hour frame. . . . .	24
15	Salinity and temperature versus density . . . . .	25
16	Along-estuary density colormap of Pescadero. Distance $x$ is considered from the coast following the curvature of the estuary as the sensors are placed in Fig. 2. . . . .	26
17	Time-series of tidal height in San Francisco (blue) and Pescadero estuary water level (black) in MLLW datum, significant wave height ( $H_{SW}$ ), dominant wave period ( $T_{DW}$ ), average wave period ( $T_{AW}$ ), and the direction from which the waves at the dominant period are coming ( $dir_{DW}$ ). . . . .	26
18	Time-series of freshwater flow from Pescadero Creek. . . . .	27
19	Time-series of wind stress ( $\tau_w$ ), NM ( $\rho_{NM}$ ), ML ( $\rho_{ML}$ ), and DC ( $\rho_{ML}$ ) densities in different depths, where sensor 1 is the deepest and sensor 4 is the shallowest (The positions in the water column of the sensors are shown in Fig. 16), significant wave height in Halfmoon Bay in blue ( $H_{sw}$ ), Pescadero estuary water level (black) and tidal height in San Francisco (gray) in MLLW datum, and freshwater inflow of Pescadero creek ( $Q$ ). . . . .	28

20	Time-series of wind stress ( $\tau_w$ ), depth wavelet frequency analysis at DC, standardized depth ( $\hat{H}$ ) in DC, NM, and ML locations, the change of the water level in a 10-hour frame ( $dh/dt$ ), standardized depth change between locations DC and ML ( $(\hat{H}_{DC} - \hat{H}_{ML})/\Delta x$ ), significant wave height in Halfmoon Bay (blue), Pescadero estuary water level (black) and tidal height in San Francisco (gray) in MLLW datum, and freshwater inflow of Pescadero creek ( $Q$ ). . . . .	30
21	Time-series of wind stress ( $\tau_w$ ), and potential energy anomaly ( $\phi$ ). Dots are the instant when wind stress is zero. The shadowed window is when the estuary is in an open state. . . . .	31
22	Time-series of wind surface shear stress ( $\tau_w$ ), Wedderburn number ( $W$ ) where the dashed line shows $W=1$ and black and gray lines show $W$ obtained at the lower and upper part of the selected window respectively, density at the bottom (blue), middle (green), and top (yellow) of the water column in NM location ( $\rho_{nm}$ ) (see Fig. 16 for sensors positions), and colormap of density in time-space at each sensor of location NM with the black and gray line that limit the lower and upper part of the window of possible values for top layer width. The dark shadowed window is when the estuary is in the open state. Light-shadowed windows are when the upwelling events were observed. Redline is the water level, and the star indicates where the surface layer ends according to Fig. 16. . . . .	32
23	Time-series of wind shear stress at the surface ( $\tau_w$ ), surface densities in locations NM, ML, and DC ( $\rho_{top}$ ), density change between locations DC and NM at the surface ( $\frac{\rho_{DC}-\rho_{NM}}{\Delta x}$ ), and density change between surface and bottom in locations NM, ML, and DC ( $\frac{\Delta\rho}{\Delta z} [kg/m^4]$ ). . .	33
24	Time-series of: $u$ and $v$ in the vertical, averaged vertical velocity, and wind stress. . . . .	34
25	Density profiles at locations (A) NM, (B) ML and (C) DC, and (D) velocity profiles of 5 moments before, during, and after a full upwelling event, and time-series of (E) wind stress and (F) buoyancy frequency showing the plotted instants. . . . .	35
26	Time-series of wind stress ( $\tau_w$ ), depth wavelet frequency analysis at DC, standardized depth ( $\hat{H}$ ) in DC and ML locations, the change of the water level in a 2-hour frame ( $dh/dt$ ), standardized depth change between locations DC and ML ( $(\hat{H}_{DC} - \hat{H}_{ML})/\Delta x$ ) with its rolling mean, and significant wave height in Halfmoon Bay (blue), Pescadero estuary water level (black) and tidal height in San Francisco (gray) in MLLW datum. . . . .	37
27	Frequency spectra of water level fluctuations in the estuary at sites in NM, DC and ML, and of wind surface stress between 11 Feb. and 20 Feb. with a close up of the lower frequencies.	38
28	Occurrence of strong wind events in Pescadero estuary. . . . .	40
29	Time-series of wind stress ( $\tau_w$ ), along-estuary velocity in the water column, along-estuary velocity in the upper and lower layers of the ADCP range, and depth wavelet frequency analysis at DC and tidal height in San Francisco (gray). . . . .	41
30	Scheme of the pycnocline tilt in an idealized estuary with the detected ADCP range in Pescadero.	42
31	Movements of the density layers in Pescadero during the first wind event of the first period. The plots were constructed using the information given by the CTD. . . . .	43
32	Wind event that was plotted in Fig. 31 with the instants of each plot. . . . .	44
33	Discharge versus estuary height and discharge versus the height change in a 10-hour-frame for the period between 11 Feb. and 20 Feb.. . . . .	45
34	Time-series of wind stress ( $\tau_w$ ), standardized depth ( $\hat{H}$ ) in DC, NM, and ML locations, depth wavelet frequency analysis at DC, the potential energy anomaly ( $\phi$ ), significant wave height in Halfmoon Bay (blue), and tidal height in San Francisco (gray), and freshwater discharge ( $Q$ ). . .	46
35	Tide level ( $\eta$ ) versus significant wave height ( $H_{SW}$ ), dominant wave period ( $T_{DW}$ ), and dominant wave period direction ( $dir_{DW}$ ) with the water level of Pescadero (Depth PDO) in colors, during the period between 11 Feb. and 20 Feb.. Four wave overtopping events were selected as the most prominent of the period and were marked in the plot with reddish stars.	47

## List of Tables

## 1 Introduction

Estuaries are geological formations that mark the interface between riverine and oceanic environments. These coastal waterbodies such as fjords, bar-built estuaries, and coastal lagoons are constantly exposed to anthropogenic or natural disturbances due to their productive importance (Schernewski, 2002; Martínez et al., 2007) and global changes (Winckler et al., 2020). These ecosystems are exposed to sea-level rise, changing precipitation, and temperature patterns, in addition to a growing human population that is largely concentrated near the coast (Neumann et al., 2015). This type of habitat is highly variable and dynamic and is where complex physical and biochemical processes take place.

Bar-Built estuaries are systems characterized by periodic/intermittently inlet closure through a sand bar (Whitfield and Bate, 2007). These are mainly found in Mediterranean climates such as Chile, California, South Africa, and Australia (McSweeney et al., 2017). Closure occurs when a sand berm forms in the entrance channel and it can occur both seasonally or irregularly throughout the year (Behrens et al., 2013). However, it is common that annual variability dominates closure events due to the marked seasonal cycles for rain and river flow observed in this type of climate (Ranasinghe and Pattiarchi, 2003). Despite the variable nature of these systems, they are vital for many species that have adapted to take advantage of the closed-mouth condition (Viaroli et al., 2008).

When the estuary inlet closes, external factors like wind, river flow, and wave overtopping can impact its structure. This could be causing changes in the density due to fresh and saltwater input or surface stress by wind effects, causing upwelling, mixing, or circulation changing the estuarine ecosystem (Ranasinghe and Pattiarchi, 1999). The wind is the main external factor present, but the stratification makes it difficult to energize the denser layer, leading in some cases to a suppression of the turbulence under the pycnocline (Cousins et al., 2010). The aforementioned makes these systems highly dynamic due to their variability in temperature and salinity, where complex physical and biogeochemical processes of oceanic and freshwater environments interact. Species that inhabit these types of environments are vulnerable to conditions such as hypoxia or anoxia in the lower layers (Kelly et al., 2018) or the retention of nutrients in the bottom (Cousins et al., 2010) and when there is upwelling or mixing it could happen abrupt changes for marine life and generate them some problems or even death (Martí-Cardona et al., 2008).

Previous research has examined the impact of wind-induced shear stress on large thermal-stratified lakes, as demonstrated by studies conducted by Coman and Wells (2012), Laval et al. (2008), and Avalos Cueva et al. (2019). These studies have investigated the influence of wind stress, particularly in instances where they occur in timescales that are comparable to their natural oscillations. They have also identified the occurrence of upwelling events triggered by the wind, which in turn results in temperature variability. However, there is a dearth of information on the hydrodynamic effects of wind in smaller saline-stratified lagoons, and it would be interesting to explore this further to gain insights into the impact of wind on their behavior and structure.

This type of estuary is widely spread in Chile's mediterranean regions, which seasonal conditions are similar to those of other places, already mentioned, where they are found, and despite this, there are few studies carried out in the country on the subject. In Dussaillant et al. (2009) an investigation was carried out on the Yali reserve, one of the most important wetlands in the central zone of Chile, whose knowledge must be complemented to fully understand the small bar-built coastal systems.

## 1.1 The Pescadero estuary

Pescadero Estuary is a small and highly stratified bar-built estuary located at the confluence of Pescadero Creek and Butano Creek on the California coast. It is located 60 [km] south of San Francisco Bay and 40 [km] north of Monterrey Bay (Fig. 1). The Mediterranean hydroclimate of Pescadero is characterized by an average annual rainfall of 750 [mm] with a cooler and more pronounced wet season that extends from November to April and a warmer dry season from May to October (Largier et al., 2015). Hydrodynamic processes in Pescadero are comparable to similar estuaries along the western coast of the Americas as well as in Australia, South Africa, and in estuaries in Mediterranean climates on the Atlantic west coast of Europe, as well as in shallow sandy inlets elsewhere.



Figure 1: Location of Pescadero Estuary on California’s Coastline. Images reprocessed from Google Earth.

The sand barrier placed at the inlet of Pescadero closes the estuary from the sea, changing its behavior to a stratified lagoon which usually happens during the dry summer season (Williams, 2014). Inlet rupture usually occurs during the wet season when precipitation increases flow and the lagoon fills to overflowing, leading to the scour of a new channel between the lagoon and the return of tidal action and seawater intrusions to the estuary (Largier et al., 2015). During periods when the mouth of the estuary is closed, the water level of the lagoon rises and could flood the surrounding marshy land.

This site holds significant importance due to several factors. Firstly, the detection of fish kills following the breaching of the lagoon mouth after a prolonged closure, as identified in the research conducted by Largier et al. (2015). Additionally, the surrounding agricultural lands hold significant productive value for the local community. However, the area also presents a few concerns, such as the risk of winter flooding in low-lying lands, which includes some roads and parts of the town. Another factor is the presence of a wide diversity of habitats and microhabitats in the estuary, which require careful monitoring and management to preserve their

ecological balance.

Pescadero has two main water inputs: freshwater inflow and saline water, which sometimes get mixed and other times form a two-layer structure. The behavior of the estuary depends on the mouth state, where we can observe an 'open' and 'closed' state. Pescadero receives freshwater inflow from two relatively small watersheds, which have a highly variable discharge, following precipitation that varies from day to day through the wet season, as well as seasonally and between years (Largier et al., 2015). The Pescadero watershed is about twice the size of the Butano watershed, and produces 57% of the streamflow (Williams, 2014). The Northern Californian coast experiences a semidiurnal tide with a neap tide range of under 1 m and a spring tide range up to almost 3 m (Williams, 2014). Saltwater gets into the estuary easily during open state, but when the inlet is closed seawater has to overtop the sandbar to get into the estuary, which happens occasionally during high tide and strong waves.

## 1.2 Motivation

In its state of disconnection from the ocean (i.e., closed state), a bar-built estuary can take the form of a shallow stratified lagoon, due to the presence of saltwater and freshwater from fluvial inputs (Behrens et al., 2016). This estuary state could lead to eutrophication if there are no energy inputs to the system (Nunes and Adams, 2014), and usually, the wind is the main source, driving mixing and destratification in small bar-built estuaries (Gale et al., 2006) triggering processes that impact mixing and circulation, which could affect the marine life of the estuary (Marti-Cardona et al., 2008).

In cases where stratification is strong, it can create a barrier, known as the pycnocline, between the denser and lighter layers of water. This pycnocline acts as a barrier that suppresses turbulence and mixing below it, making it difficult to energize and mix the denser layer with the lighter layer. As a result, the denser layer remains stratified and separated from the lighter layer, leading to a lack of vertical mixing and exchange between the layers (Cousins et al., 2010). This phenomenon can occur in various water bodies, including estuaries, lakes, and oceans, and has implications for the distribution of nutrients, oxygen (Kelly et al., 2018), and other properties within the water column, which can impact the overall ecosystem dynamics and health of the water body (Marti-Cardona et al., 2008).

These waterbodies are highly dynamic, so it is crucial to understand the mixing and stratification dynamics of aquatic systems. Estuaries are the connection between the earth and the ocean, receiving waters coming from rivers and creeks that are exposed to anthropogenic effects, causing changes in freshwater flow or temperature, in addition, to being subjected to sea level rise and wave climate variations (Winckler et al., 2020; Holt et al., 2010; Thorne et al., 2021). Besides, in the estuaries, of their contact with the coast and rivers, activities such as fish farming or agriculture are developed, so they have economic and social importance to communities.

## 2 Objectives

### 2.1 General objective

The main goal of the present work is to comprehensively understand and quantify the drivers of stratification and mixing in closed bar-built estuaries. These estuaries are characterized by a mouth that is periodically closed by sandbars, leading to unique hydrodynamic conditions. By investigating and analyzing the factors

that influence stratification and mixing in such estuarine systems, this research aims to provide insights into the physical processes that govern water column structure and dynamics in these environments. The findings of this study will contribute to a deeper understanding of how external forces, such as wind stress, freshwater input, and wave overtopping, interact with the complex estuarine morphology to influence stratification and mixing patterns. This knowledge will have practical implications for the management and conservation of closed bar-built estuaries, as it can inform decision-making related to water quality, ecosystem health, and coastal resource management. Our case study is the Pescadero Estuary, a bar-built estuary in California that represents many other small inlet systems in mediterranean climates worldwide.

## 2.2 Specific objectives

The specific objectives of this study are:

- (1) To investigate the velocity and density variability in a small, highly stratified estuary during its closed state. The findings will contribute to our understanding of water column dynamics in closed bar-built estuaries.
- (2) To identify the influence of wind stress on the hydrodynamics of a closed bar-built estuary. This research will contribute to a better understanding of the relationship between wind stress and estuarine stratification.
- (3) To study the wind-estuary interaction and the effects of other external factors such as water inflow and wave overtopping. This is crucial for understanding the dynamics of estuarine stratification and mixing, which have significant implications for water quality, ecosystem health, and resource management.

## 3 Literature review

### 3.1 Bar-built estuaries in the ecosystem and the community

Climate change is affecting multiple marine ecosystems globally (Hewitt et al., 2016). Its been detected that the global oceanic oxygen content has decreased during the last five decades (Schmidtko et al., 2017) and that air temperature is increasing in oceans (Omstedt et al., 2004; Jones et al., 1999). Some studies expect that the absolute mean sea level on Chilean coasts rises between 0.35 to 0.74 m in the next 80 years (Winckler Grez et al., 2020). The effects of climate change can put at risk the coastal zones, including estuaries and coastal lagoons which are especially abundant ecosystems in flora and fauna.

In addition, there is evidence that there is a decrease in surface wind speeds in Northern Europe (Woolway et al., 2017) and an increase in along-shore winds in the Chilean coastal zone (Winckler Grez et al., 2020). It is known that changes in surface wind speed affect the number of days that a lake is stratified, which affects the nutrient availability and quality of a waterbody, changing the amount of oxygen present in deep waters (Woolway et al., 2017). It is important to study wind effects in estuaries to be able to quantify how wind-speed changes will affect these environments.

In central Chile, there is a decrease in river discharges affecting buoyancy and stratification (Winckler Grez et al., 2020), which can be causing a wide range of changes in estuarine and marine ecosystems, including changes in oxygen availability. These changes can impact fish populations and other autotrophic organisms.

The importance of intermittently closed estuaries goes beyond local impacts. These estuaries can accumulate sediment while the inlet is closed (Thorne et al., 2021), and in rainy seasons they open their mouth naturally because of the increase in freshwater inflow (Hoeksema et al., 2018). This process settles sediments to the nearby marshes helping to maintain their elevation according to the sea level, mitigating the consequences of sea level rise (Thorne et al., 2021). The mouth, maybe, is exposed to artificial openings to avoid flooding the surrounding lands (Behrens et al., 2013), which does not allow the sediments to set in the marsh platform (Thorne et al., 2021), not allowing them to keep their normal elevation that protects the coastal zone from the sea level.

Increased river discharge due to climate change could lead to increase erosion and the number of suspended particles of sediment in the water (Whitfield and Wooldridge, 1994). Enhanced sediment concentration could lead to accumulation in the estuary, changing the equilibrium of opened and closed state of the sand bar, which along with the increase of freshwater input could flood the surrounding land, and decreased discharge could do the opposite (Peeters and Kipfer, 2009). Consequently, depending on the vegetation present and its oxygen demand, deep-water oxygen may be reduced or suppressed (Kelly et al., 2018; Largier, 2021). Also, the density of the surface waters will be reduced and thus could change the estuary behavior to external factors such as wind stress.

Bar-built estuaries are under continuous anthropogenic stress due to their closeness to human settlements (Clark and O'Connor, 2019) and their productive importance. Dams constructed upstream for water storage reduce the freshwater that goes to the ocean, causing the retention of suspended sediments. This results in a change in the morphology of the estuary due to not receiving the sediments that used to accumulate in the inlet, leading to premature scour of the sand bar (Peeters and Kipfer, 2009). Also, to prevent flooding of roads or agricultural lands nearby, the community plan the opening of the inlet artificially, which could result on abrupt changes on the estuary ecosystem Behrens et al. (2013).

### 3.2 How bar-built estuaries are studied in Chile and around the world

McSweeney et al. (2017) studied the bar-built estuaries all around the world and their climatic, marine, and fluvial conditions to classify them and quantify the drivers of their distribution in each continent. That let the estuary response to climate change and human impacts to be estimative and include integrated coastal management, reducing impact in the environment.

Dussaillant et al. (2009) studied a Chilean coastal lagoon in its open and closed state and observed that in its closed state the rainfall influence was not important except for the storms that open the inlet to the sea. He also observed that wind effects can be important during the disconnected phase to the ocean, producing a slope in the lagoon levels. He studied the connected phase using a general pattern, spectral, and Fourier analysis.

In their study, Gale et al. (2006) investigated the dynamics of Intermittently Closed and Open Lakes and Lagoons (ICOLLS) during their closed state. The research findings revealed that the presence of stratification ( $N > 0.1 s^{-1}$ ) can lead to depletion of oxygen in the bottom waters. This particular factor has been associated with fish kills in Pescadero, as documented by (Largier et al., 2015).

Kelly et al. (2018) conducted a study on Lough Furnace, Ireland, a naturally deep saline lagoon characterized by restricted tidal inflows and long periods of low freshwater input, which showed continuous vertical stratifi-

cation and anoxia in the lower layers. The study found that specific tidal events and wind-driven upwelling could oxygenate the deeper layers, revealing a correlation between tidal influence and wind stress in vertical mixing.

Behrens et al. (2016) observed the salt intrusion in a bar-built estuary and its differences between closed and open state conditions. The study found the presence of alternating shallow sills and deep pools, which act to trap the salt after intrusion, and suggested that internal seiche motions in the outer estuary initiate the intrusion by lifting saline water in the pycnocline high enough to crest the sills. This salinity intrusion extends to distances of several kilometers from the beach when the estuary is in closed state.

In Rodeo Lagoon, a shallow strongly-stratified lagoon, (Cousins et al., 2010) investigated the effect of stratification on water column parameters such as salinity, dissolved oxygen, and nutrient levels. They found that stratification causes a significant suppression of turbulence below the pycnocline, resulting in the confinement of nutrients in the lower layer for several months. The study revealed that wind is the primary source of mixing in the lagoon, and destratification by wind allows for the redistribution of nutrients from the bottom brackish layer.

### 3.3 Hydrodynamics of a stratified waterbody

In nature, stratified waterbodies can be found not only in estuaries (Human et al., 2016) but also in lakes (Valerio et al., 2012; Imam et al., 2013; Coman and Wells, 2012), coastal lagoons (Cousins et al., 2010) and also in oceans: continental shelf seas, river plumes, etc. Although lakes are usually studied as thermally stratified water systems, they exhibit comparable hydrodynamics to thermal-haline stratified coastal waterbodies. In estuaries, when the tidal connection with the ocean is limited, water circulation is driven by wind and freshwater inflow, resulting in similar dynamics to lakes in a smaller scale.

In stratified lakes or estuaries, it is common to find a two-layered system with the presence of an interface of finite thickness, which is a third middle layer. This middle layer can be observed as a gradient of density or temperature that separates the upper layer from the lower layer. The interface layer thickness is an important parameter that can impact the dynamics of the water column in these types of waterbodies (Simpson and Hunter, 1974).

Depending on the strength and duration of wind forcing, the lake or estuary can manifest an upwelling response. Upwelling is a significant process that occurs in stratified estuaries and lakes, influencing their hydrodynamics and ecosystem dynamics. It involves the vertical transport of nutrient-rich, deep oceanic waters to the surface, promoting enhanced biological productivity and supporting diverse marine ecosystems (Gupta et al., 2022). One parameter commonly used to characterize upwelling in estuaries is the Wedderburn number (Imberger and Hamblin, 1982). By quantifying the Wedderburn number, researchers can assess the strength and effectiveness of upwelling processes in bar-built estuaries, aiding in the understanding and management of these dynamic coastal environments.

The wind's energy is the primary source of energy for the water column's circulation, and it can cause an upwelling response when it is strong enough to overcome the stratification of the water layers. Upwelling occurs when the wind's energy forces the lower layer of water to move upward, bringing nutrients and other materials to the surface that can stimulate primary productivity in the water column (MacIntyre et al., 2010).

Roberts et al. (2021) studied the setup and relaxation of spring upwelling in a deep, rotationally influenced lake, Lake Tahoe, using a combination of field observations and numerical modeling to investigate the mechanisms that cause the upwelling of deep water in the lake. They found that the setup of upwelling was caused by the wind-induced mixing of the upper layer of the lake, which resulted in a deeper mixed layer and the buildup of potential energy. The relaxation of upwelling occurred when the wind stopped, and the potential energy was converted into kinetic energy, which led to the downwelling of surface water. These findings provide new insights into the mechanisms that control the dynamics of upwelling in deep lakes and could help inform the management of these ecosystems.

The Wedderburn number was designed for rectangular basins, but this approach is not too close to reality, where basins can be of multiple and irregular shapes. Shintani et al. (2010) used a numerical model to demonstrate that the upwelling of deep water in lakes with any geometry can be described using the Wedderburn number as a function of the Richardson number, the buoyancy frequency, and the Rossby number. This Wedderburn number is not a detailed estimate of the interface behavior, therefore provides a scale for the seiching. These results provide a better understanding of the physical processes that drive the upwelling of deep water in lakes and could help improve the management of these ecosystems.

Wind stress also induces a tilting of at the interface between layers of different densities. This interface tilt results in the transfer of momentum from the wind to the water column, leading to mixing and vertical exchange processes. The tilt can be quantified with the internal wave period  $T_1$ , and also we can consider that after commencement of the wind stress, it takes  $T_1/4$  for the condition identified by W to occur.

Monismith (1985) discussed that a three-layered fluid has a similar behavior as a two-layered fluid when the upper layer is shallow. This is because the shallow upper layer behaves like a mixed layer, while the middle layer acts as an interface layer separating the mixed layer from the lower layer. When the upper layer accelerates due to a wind forcing in the surface, the mixed layer starts to deepen rapidly, while the upper layer tilts and might upwell (Monismith et al., 2006).

The response of stratified lakes or estuaries to wind forcing events can be complex, involving interactions between the layers of the water column, upwelling responses, and changes in the water column's stability (Jayaweera et al., 2019). Upwelling occurs when the wind's energy forces the lower layer of water to move upward, bringing nutrients and other materials to the surface that can stimulate primary productivity in the water column (Bastidas et al., 2021). The thickness of the interface layer is an important parameter that can impact the dynamics of the water column in these types of waterbodies (Xu et al., 2017). Factors such as wind strength and duration, water temperature, and the presence of nutrient-rich layers in the water column can all affect the response of stratified lakes or estuaries to wind forcing events (Nidheesh et al., 2018).

### 3.4 Pescadero estuary studies

Recent studies on the Pescadero Estuary have focused on fish kills that occur when the sandbar closes, leading to the creation of an anaerobic environment in the bottom waters (Sloan, 2006). Geochemical analysis of sediments has shown that the transition from the closed to open state leads to poor water conditions within the Pescadero Estuary, with many indicators reaching values outside the range of optimal conditions for fish or aquatic life (Richards et al., 2018). Huber and Carlson (2020) documented one of the breach-induced fish kills events, demonstrating a case of ecosystem function loss caused by chronic degradation of water quality during the closed estuarine state. While previous literature on the Pescadero Estuary has focused

on management plans for biological productivity (Curry et al., 1985) or preserving the hydrology of the estuary (Williams et al., 1990), these recent studies highlight the importance of understanding the physical and chemical dynamics of bar-built estuaries.

In addition to the effects of sandbar closure, physical phenomena such as the effects of the constriction generated by the mouth in its open state have been studied. Williams and Stacey (2016) observed that wave setup and tides set the estuarine water level, while the mouth sandbar limits ocean gravity waves from entering the estuary but permits infragravity motions to pass through the inlet, inducing energetically important high velocities. These studies highlight the strong dependence of hydrodynamics of small bar-built estuaries on nearshore processes and the need to understand the complex interactions between external factors and estuary dynamics.

## 4 Methods

### 4.1 Field measurements

Four field campaigns were carried out between 2010 and 2012 described in the work of Williams (2014) and Williams and Stacey (2016). This work focus exclusively on the data between January and March 2012 to analyze the behavior of the estuary in a closed state. Measurements were made in the estuary using instruments for velocity and depth, as well as a meteorological station to collect wind speed and direction data in the marsh.

Depth data were collected using moored Conductivity, Temperature, Depth sensors (RBR XR-420 CTD) placed at different heights and distributed along the estuary at four locations as shown in Fig. 2: Near Mouth (NM), Mid-Lagoon (ML), Deep Channel (DC), and Pescadero Creek (PC). It should be noted that the instruments placed along the water column are floating, so they have range of motion in the vertical (Fig. 3). The estimated difference in the instruments depth between DC and the others is of 0.8 m for NM, 0.75 m for ML and 0.7 for PC. We have to consider that the instruments PC and NM were moved in February 16th, so we estimated the value after that day.

Density profiles were made on 16 Feb. with a CTD logger around 5 p.m. at the locations indicated in Fig. 2. The moment the profiles were made the wind was calm, so is not causing a disturbance in the water.

Velocity measurements were made with an Acoustic Doppler Current Profiler (ADCP 1200 KHz WH) anchored to the bottom of the estuary at location DC. This instrument is designed to be used in deeper water, so data collected from the surface could be affected by the interference caused by reflection. Also, this instrument, despite it is on the location DC, does not have the same depth than the CTD moored at the same location, due to the bathymetry (See diagram of Fig. 2).

For wind speed data, an anemometer (Model #05106, RM Young Fig. 4) was installed 3 m above the water level in marshy land adjacent to the estuary (Fig. 2). All the information of the instruments are summarized in Table 1.

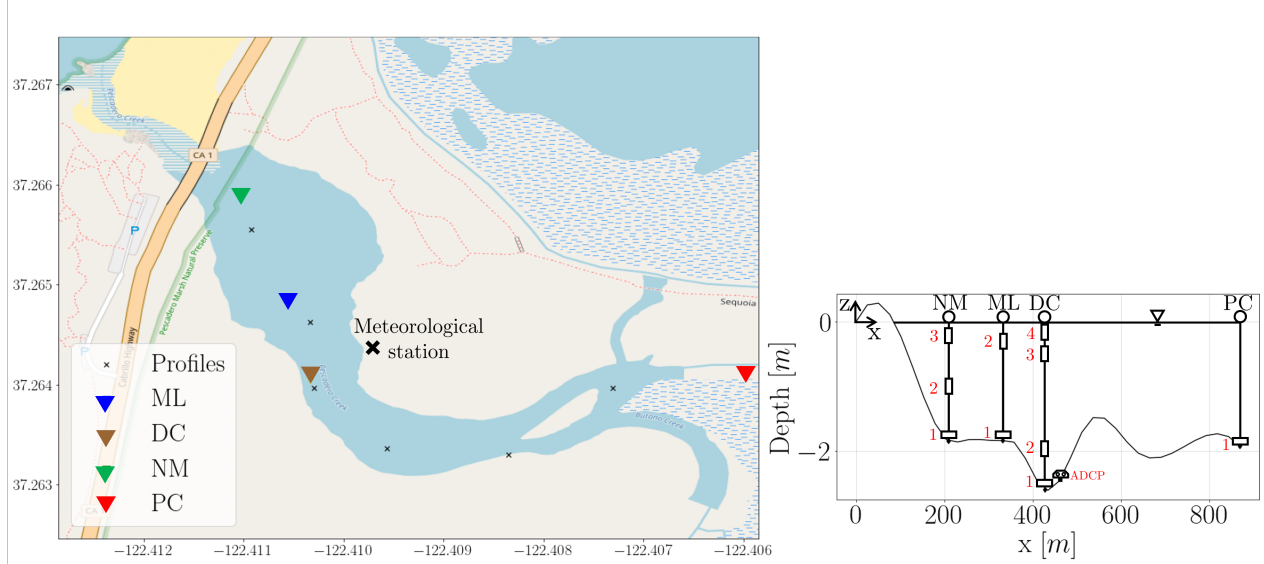


Figure 2: Pescadero estuary map and location of the moorings (NM: Near Mouth, ML: Mid-Lagoon, DC: Deep Channel and, PC: Pescadero Creek), meteorological station. Profile locations for CTD measurements in Fig. 2 are indicated by small "x". Diagram of the elevation view of Pescadero in the along-estuary direction with the locations of the sensors in the water column.

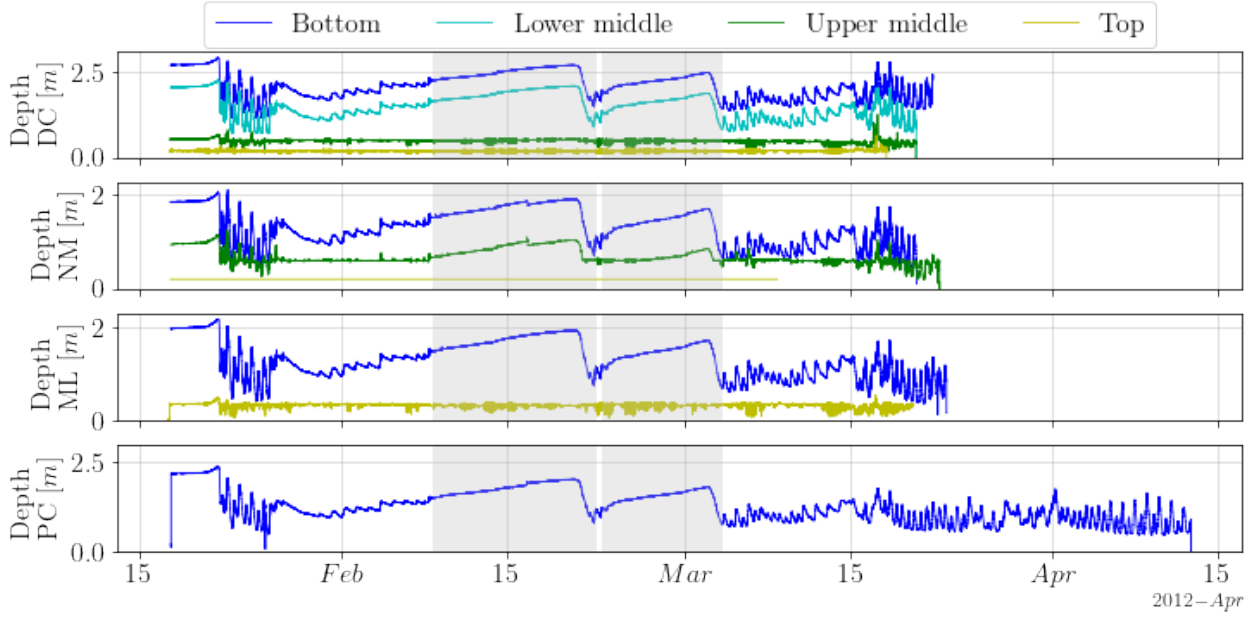


Figure 3: Time-series of instruments depth in all locations. The windowed data is the used in this study.

## 4.2 External data

To complete the information, the freshwater streamflow into the Pescadero estuary is estimated based on a United States Geological Survey (USGS) gauge located on Pescadero Creek 8.5 km upstream from the estuary mouth (USGS 11162500). As the Butano creek is also contributing, the total discharge estimation given by



Figure 4: Anemometer for wind measurements. Model #05106, RM Young. (Williams, 2014)

Table 1: Information of the instruments used in the field campaign.

Location		Instrument	Sampling Rate	Height above bed	Dates of data
NM	1	RBR XR-420 CTD	10 s	0 cm	17/01/2012 - 20/03/2012
	2	RBR XR-420 CTD	30 s	50 cm - 90 cm	17/01/2012 - 22/03/2012
	3	RBR XR-420 CTD	30 s	75 cm - 1.7 m	17/01/2012 - 08/03/2012
DC	1	RBR XR-420 CTD	10 s	0 cm	17/01/2012 - 21/03/2012
	2	RBR XR-420 CTD	10 s	50 cm - 80 cm	17/01/2012 - 20/03/2012
	3	RBR XR-420 CTD	10 s	1 m - 2 m	17/01/2012 - 20/03/2012
	4	RBR XR-420 CTD	10 s	1.3 m - 2.6 m	17/01/2012 - 18/03/2012
	1	ADCP	2 Hz	0 m	16/02/2012 - 14/03/2012
ML	1	RBR XR-420 CTD	10 s	0 cm	17/01/2012 - 20/03/2012
	2	RBR XR-420 CTD	10 s	40 cm - 1.6 m	17/01/2012 - 23/03/2012
PC	1	RBR XR-420 CTD	30 s	0 cm	17/01/2012 - 12/04/2012
Profiles		RBR CTD	6 Hz	-	16/02/2012
Met. station		Model # 05106, RM Young	6 min	-	27/10/2011 - 19/04/2012

Williams (2014) is  $Q_T = 1.76 Q_{P,C}$ .

The tide height data in San Francisco Bay and Monterrey Bay (stations 9414290 and 9413450 respectively) were obtained from the National Oceanographic and Atmospheric Administration (NOAA). Wave climate data were obtained from the National Data Buoy Center, 40 km offshore from the coast of Half Moon Bay (station 46012) (Fig. 5).

### 4.3 Data processing

#### 4.3.1 Salinity and temperature

The CTDs measurements were made with a frequency of 10 or 30 sec, and at each location, there were one (PC), two (ML), three (NM), or four (DC) instruments at different depths (Table 1). The bottom pressure measurements at each sensor were corrected for sea-level atmospheric pressure measured at the nearest weather station located at the Half Moon Bay airport. This work focuses exclusively on the two periods where



Figure 5: Stations and sites locations of the external data obtained for this study.

the estuary is closed between February and March.

We subjected the data to quality control, where data from the beginning and end, when the instrument was out of the water, and some data in the middle, where we observed time jumps incompatible with reality, were eliminated. Density is calculated from salinity, temperature, and pressure data, by the GSW Python package which is an implementation of the Thermodynamic Equation of Seawater (TEOS-2010).

Additionally, CTD profiles were made on February 16th, between 17:00 and 17:30 which were used to calculate the density also using TEOS-2010. When the profiles were taken the wind was very calm so we can say that the estuary was not having any significant external forcing.

#### 4.3.2 Water velocity

Velocity data collected with the ADCP in its raw form is composed of different points measured throughout the water column (bin), which were in instrument coordinates. Some of this bins were measured out of the water.

First, we removed the bins above the surface from the record and then rotated them to earth coordinates (East, North) using the method shown in Teledyne (2008). On the other hand, the ADCP has a blank space of measures at the bottom, so the first measured point was 71 cm above the ground, meaning there is only a window of velocity data in the water column (Fig. 6).

The velocity data obtained from the ADCP, considering all bins that weren't deleted, was processed using an axis-rotation technique to align the measurements with the principal coordinates ( $u, v$ ). This transformation was performed based on the direction of maximum variance, as illustrated in Fig. 7. The data analysis covered the period from 17 February to 9 March, which encompassed two observed breaches of the estuary mouth, as depicted in Fig. 6. The inclusion of these inlet openings was essential to capture the inflow direction during estuary draining events. The principal direction angle was determined to be  $48.6^\circ$  clockwise from the west axis, and it was established that the positive velocity component ( $u$ ) corresponded to the flow direction towards the sea.

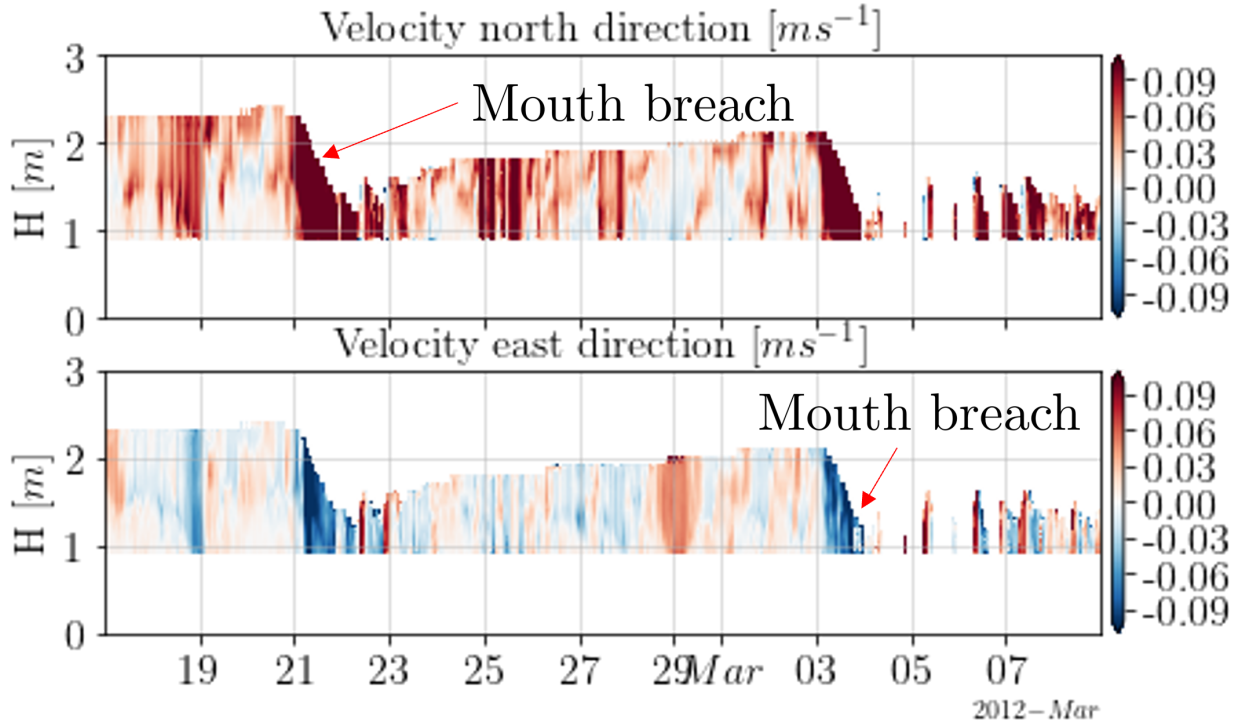


Figure 6: Timeseries of velocity data plotted in North and East directions in the water column.

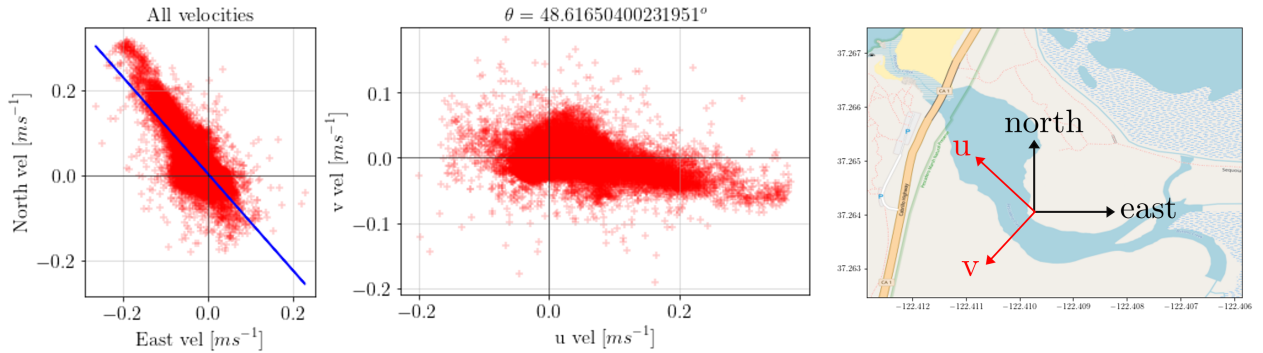


Figure 7: Velocity data plotted in North-East and  $u - v$  coordinates, and a map of Pescadero signaling the coordinates.

We averaged ADCP data every 5 minutes to remove high-frequency signals. However, CTD data at the DC location was not at the same depth due to bathymetry so, we estimated the difference between both and adjusted the first cell to 0.91 m above the bottom of the estuary.

#### 4.3.3 Wind velocity

Raw wind data contained the velocity magnitude and direction as shown in Fig. 8. Wind velocity coordinates were transformed first in east-north coordinates. Then, the data were also axis-rotated to the principal coordinates of the estuary currents, with an angle of  $48.6^\circ$ .

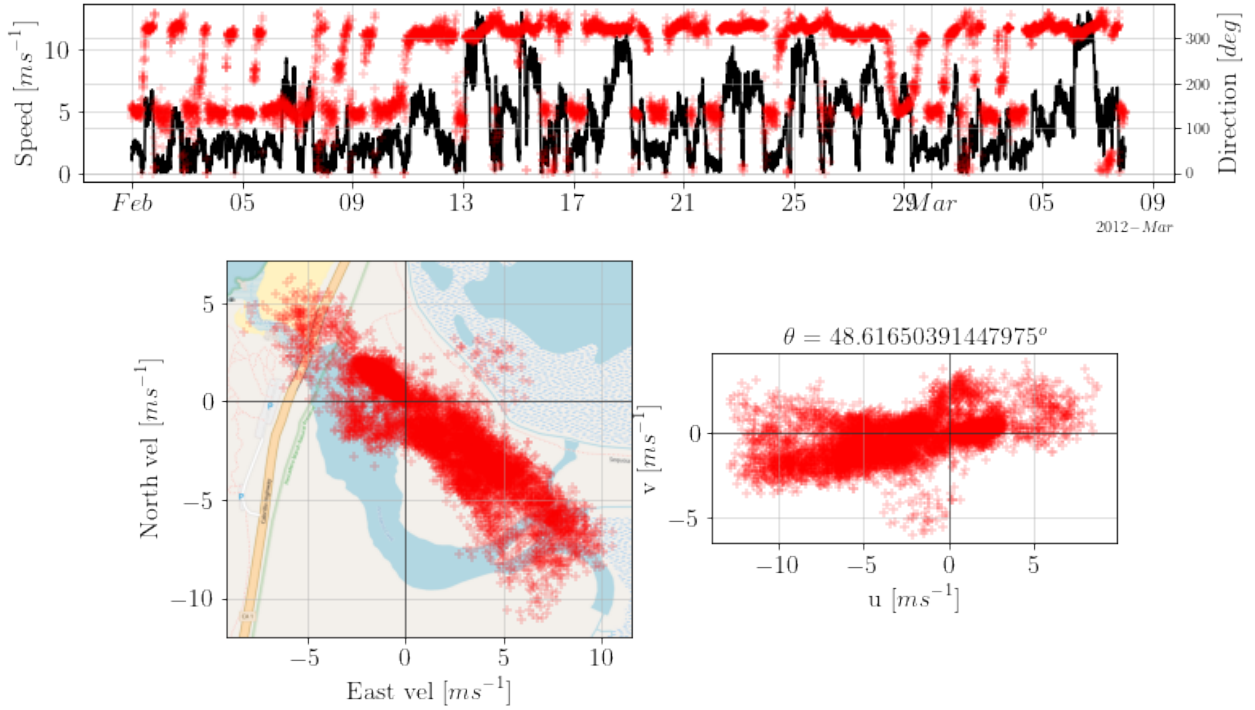


Figure 8: Time-series of wind velocity magnitude and direction. Wind velocity in North-East coordinates over the Pescadero map and in (u,v) coordinates.

## 4.4 Analysis techniques

### 4.4.1 Stratification

To represent stratification we used buoyancy frequency, defined as (Kundu et al., 2015):

$$N^2 = -(g/\rho)(\partial\rho/\partial z) \quad (1)$$

where  $\rho$  is the density of the fluid,  $g$  is  $9.81 m/s^2$  and  $z$  is the depth. This equation is representing the water column stability, which increases or decreases as the fluid is more or less stratified. The potential energy anomaly was calculated to observe the behavior of density in the water column. It represents the work per volume required to completely mix the water column and is calculated using the equation shown by Simpson et al. (1985):

$$\phi = \frac{1}{h} \int_0^h (\bar{\rho} - \rho) g z dz \quad (2)$$

where  $h$  is the total depth, and which we discretized according to the number of sensors that each location had and considering each layer's limits as the corresponding upper and lower sensors and the density for the whole layer as the upper one. We employed the potential energy anomaly ( $\phi$ ) as a diagnostic tool to assess the stratification of the water column before and after a wind event, thereby characterizing the state of the water column under conditions of zero wind stress and investigating the presence of mixing. Furthermore, we calculated the buoyancy frequency ( $N^2$ ) during wind events to examine its relationship with density and velocity profiles.

#### 4.4.2 Wind stress

The wind shear stress was calculated following Read et al. (2011):

$$\tau = \rho_{air} C_D U_{10}^2 \quad (3)$$

Where  $\rho_{air}$  is the specific weight of air ( $1.2 \text{ kg/m}^3$ ) and  $C_D$ , the drag coefficient, as defined by Large and Pond (1981), was set at 0.0012 for wind velocities ranging from 4 to 11 m/s. Since the measured wind speeds in our study were below 11 m/s and the results demonstrated insensitivity to  $C_D$ , we adopted the value of 0.0012. This choice enables a direct comparison of our observations with other studies that utilized a constant  $C_D$  value, ensuring consistency across the literature.  $U_{10}$  is the adjusted wind speed at 10 meters high, and it was obtained by:

$$U_{10}^2 = U_z \left(1 - \frac{C_D}{\kappa} \ln \frac{10}{z}\right)^{-1} \quad (4)$$

with  $\kappa = 0.4$  as the Von Karmann coefficient and  $z = 3 \text{ m}$ , the height of our wind measures.

To study the response of the stratified layers to a wind impulse and identify the upwelling we used the Wedderburn number (Imberger and Hamblin, 1982):

$$W = \frac{g' h_1^2}{L u_*^2} \quad (5)$$

where we estimated  $h_1$  as the 30% of the DC's total depth (Fig. 9), L as 392 m, and for  $u_*$  and  $g'$  we used:

$$g' = \frac{\rho_{bottom} - \rho_{surface}}{\rho_{surface}} g \quad (6)$$

$$u_*^2 = \frac{\tau_w}{\rho_{surface}} \quad (7)$$

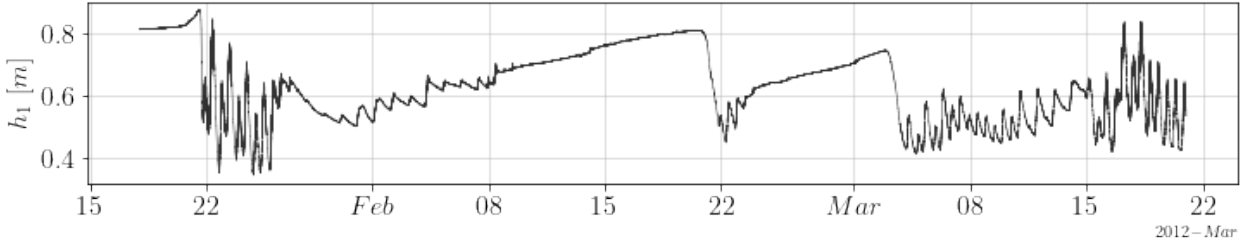


Figure 9: Time-series of 0.3 times the total depth of the estuary at the location DC.

To analyze the relationship between wind stress and density, we standardized and normalized the signals and applied cross-correlation. Cross-correlation between wind stress and density signals is used to find the time lag (phasing) between both and their level of correlation along the locations (propagation) measured in the estuary. Also, after commencement of the stress, the event of the condition identified as W takes 1/4 of the internal wave period  $T_1$  (Stevens and Imberger, 1996):

$$T_1 = \frac{2L}{\sqrt{\left(\frac{\epsilon g h_1 h_2}{h_1 + h_2}\right)}} \quad (8)$$

#### 4.4.3 Surface fluctuations analysis

To analyze what was happening on the surface, a frequency spectral analysis was carried out in order to identify the most important processes that affect the water level. First, Welch (1967) method was applied to reduce the data noise and there was applied a detrend. Finally, to obtain much clearer data and then apply the frequency spectral analysis, the signal was multiplied by a quadratic window:

$$w[n] = \left( \frac{n - N/2}{N/2} \right)^2 ; 0 \leq n \leq N \quad (9)$$

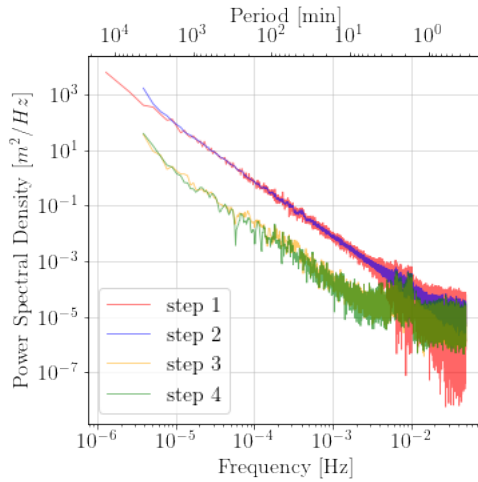


Figure 10: Step 1: Raw frequency spectral analysis. Step 2: Frequency spectral analysis with a noise reduction. Step 3: Frequency spectral analysis with a noise reduction and a detrend applied. Step 4: The obtained signal from step 3 is multiplied by a quadratic window shown in Eq. 9.

To complement this information, an analysis of the wavelet transform was carried out using the Python package PyWavelets (Lee et al., 2019). The one-dimensional continuous wavelet transform was applied to the DC surface height data using the first-order Gaussian derivative family for a period range between 10 s and 2.8 min, we limited the frequencies to highlight what is important. This, in order to identify important events and other external phenomena, such as a wave overtaking the sandbar due to high tide. This analysis delivers coefficients that are a function of scale and position and that serve as a scalogram to visualize the wavelet.

To carry out a more detailed visual analysis, the standardized heights were obtained at the NM and DC points, first applying a linear detrend and then dividing the data by the standard deviation. This is for comparing results on the same scale. All the mentioned data were plotted according to local time, to analyze visually considering the factors that affect day and night as temperature and wind.

## 5 Results

The Pescadero Estuary, located at the confluence of Pescadero Creek and Butano Creek on the California coast, is a small and highly stratified estuary. It is characterized by an intermittently opening and closing inlet, where a sandbar acts as a barrier between the estuary and the sea. During the dry season, the sandbar closes the inlet, transforming the estuary into a stratified lagoon.

Field measurements were conducted between 17 Jan. 2012 and 21 Mar. 2012, capturing the estuary's conditions during this period. The inlet was initially closed when the sensors were installed and remained closed until 21 Jan. 2012. Subsequently, the inlet closed again on 07 Feb. 2012 and reopened on 21 Feb. The estuary experienced its third closure on 24 Feb., which persisted until 3 Mar. (Fig. 11).

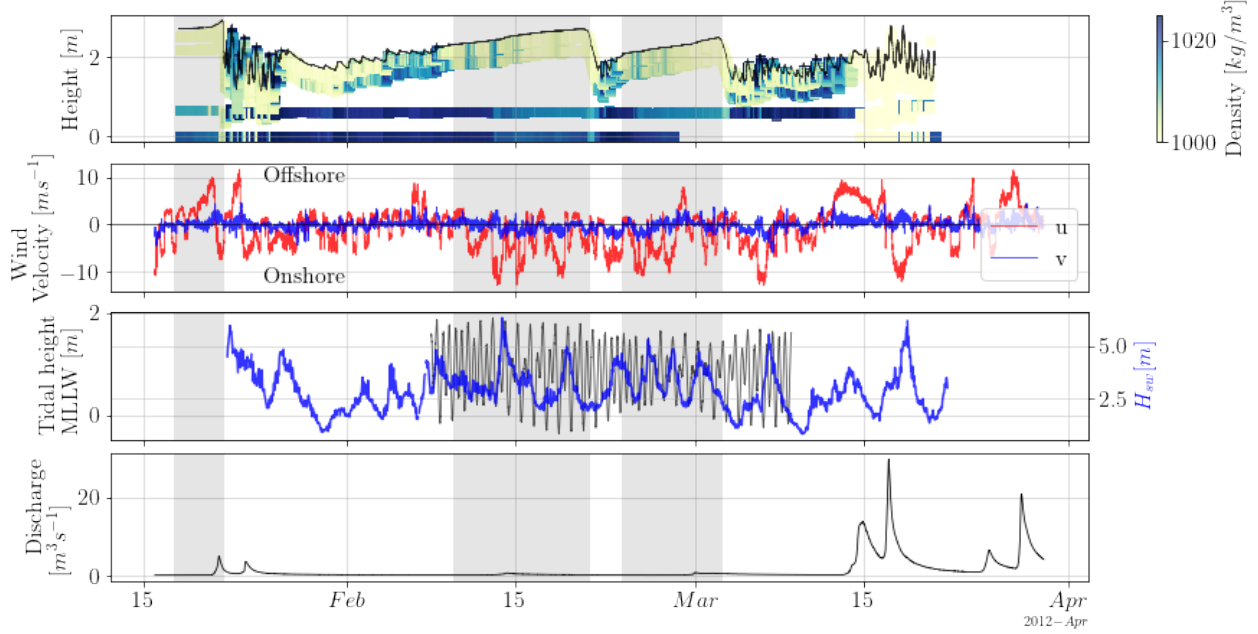


Figure 11: Time-series windowing the closed state of colormap of density in DC location in the water column height, where the black line represents the water level; wind speed in  $u$  and  $v$  direction.

When the mouth closes in Pescadero we can observe that the flow of water between the estuary and the sea is significantly reduced, almost completely blocked, causing a decrease in water exchange as we can observe in Fig. 11. This restricted exchange isolates the estuary from the influence of oceanic processes and creates a more confined waterbody. One consequence of the inlet closure is the establishment of stratification within the estuary. In the watercolumn we can observe lighter freshwater sitting atop denser saltwater.

## 5.1 Conditions observed during the closed state

Abrupt decreases in water level that were proceeded by a slow increase in the estuarine water level without tidal influence were identified as mouth openings and when tidal energy is not visible at the water level there is a mouth closure. We observed that the inlet opened three times and in each one there are abrupt density changes in the water column along with other important conditions that we are going to address below.

### 5.1.1 Wind in the estuary

In Fig. 13 we can observe that the wind is mainly bidirectional and when it goes onshore the magnitude is bigger. Directions between 300 and 360 degrees come from the ocean and the wind that blows from 100 to 170 degrees comes from inland. This form is due to the topography of Pescadero which has an escarpment at the south of the inlet, protecting the mouth. Also, the marsh itself is located in a low valley, constricting wind

flow paths. For the along-estuary velocity, ( $u$ ) we observe that the maximum velocities reach between 10 and -10 m/s approximately (Fig. 12). In the cross-estuary velocity, ( $v$ ) we observed just a few spikes where the maximum velocity was reached, at approximately 5 and -5 m/s.

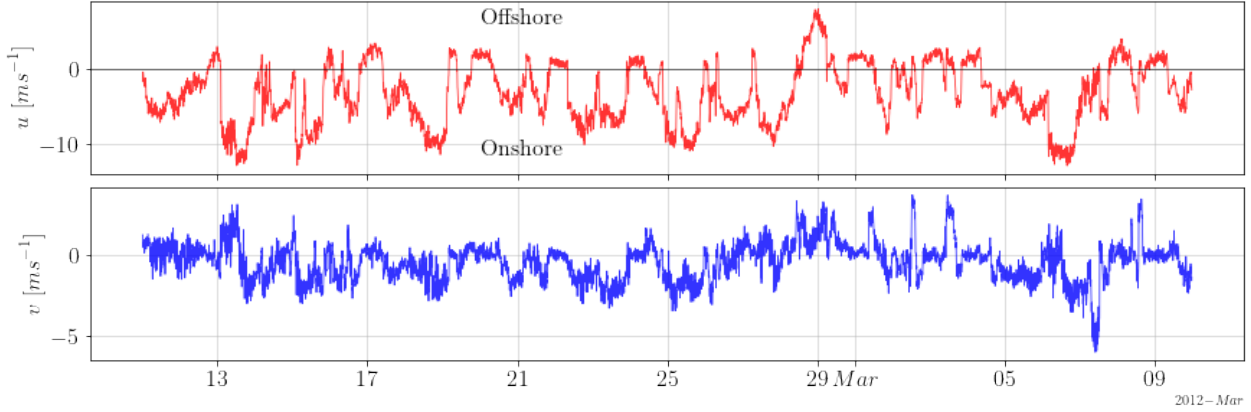


Figure 12: Time-series of wind speed in  $u$  and  $v$  direction.

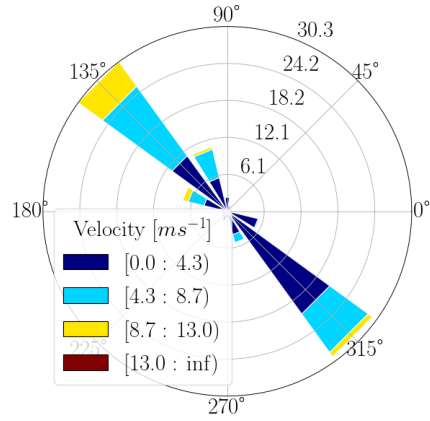


Figure 13: Windrose of the data collected in Pescadero from 15 Jan. to 20 Mar. Maximum speed registered in the studied period was 13.02 m/s

The response to strong and sustained wind stress in a closed state bar-built estuary starts with a setup of the surface and a change in the pressure gradient. This will cause the pycnocline to tilt upwards at the upwind end of the estuary leading sometimes the bottom layers to rise to the surface. The reduction or end of this wind forcing releases the pycnocline from its tilted position and return to horizontal.

The upwelling effect caused by wind forcing has potential relevance in nutrient and oxygen exchange between layers (Kelly et al., 2018) and has been studied widely in lakes using temperature measurements (Coman and Wells, 2012; de la Fuente et al., 2010; Roberts et al., 2021), however, there are fewer studies that observe this kind of behavior at bar-built estuaries or in smaller coastal lagoons.

### 5.1.2 Evolution of density structure

Pescadero estuary is characterized by having a strong thermohaline stratification in its closed state (Fig. 14). When the estuary inlet starts closing, temperature and salinity acquire different values on the top and bottom of the lagoon, increasing density change in the vertical (Largier et al., 2015). The sand bar that forms at the inlet of the estuary contains the freshwater inflow and does not allow the waves to enter, but during high tide the waves could be overtopping it (Laudier et al., 2011), contributing to the salinity in the system. This, depending on the magnitude of the intrusion, could affect the stratification of the entire estuary.

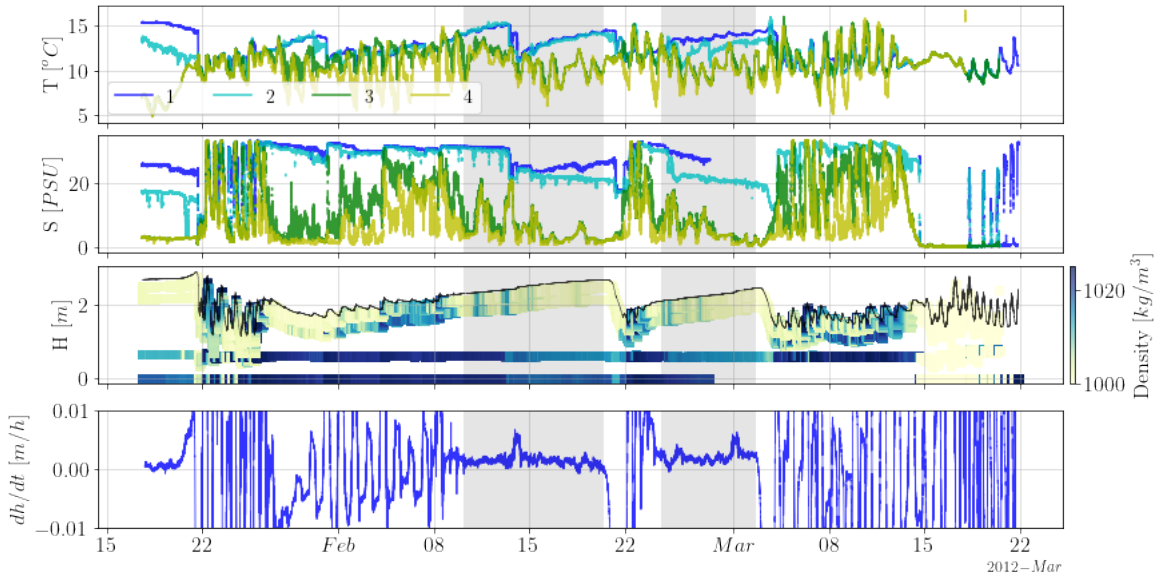


Figure 14: Time-series windowing at both closure phases of temperature and salinity in NM, where 1 is the deepest sensor and 4 the shallowest, colormap of density in NM in the water column, where the black line represents the water level, and the change of the water level in a 10-hour frame.

Temperature is an important parameter for density, notwithstanding salinity stills dominates density values, there are a few points we must aboard about temperature in Pescadero. First, horizontal temperature gradients are present in Pescadero, where upstream is warmer meaning the water coming from the creek is warmer. In addition, during the studied period, the water temperature in San Francisco buoy from the National Data Buoy Center was between 9°C and 11°C, so the water coming from the sea will be colder. Second, during closed state the temperature in the estuary is colder on the surface and warmer at the bottom, probably since is winter during the studied period and the temperature in the air is lower than in the water coming from upstream. The coldest temperature can be on the surface without sinking for being denser because salinity dominates density in this case as we can observe in Fig. 15. Third, Pescadero in its closed state takes the form of a shallow lagoon, meaning that is more prone to heat loss and air temperature than other bigger lakes (Peeters and Kipfer, 2009).

We defined the closed state at the estuary when the depth's change in time  $\Delta h/\Delta t$ , with  $\Delta t = 10$  hours, is positive and less than 0.01 m/h for more than a day (Fig. 14), meaning that the lagoon is filling with fresh water, increasing its level, and with a low influence from the sea. In that context Pescadero is in closed state three times: in mid January, in mid February, and in late February/early March where the first one is at the start of the time series, not including the initial closure, while the second and third closures are in gray shadow

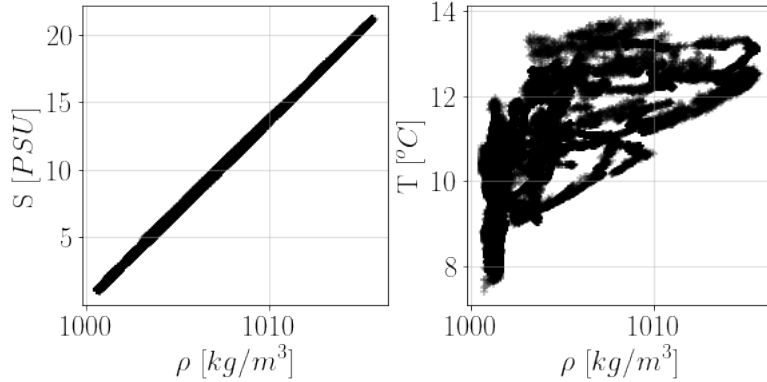


Figure 15: Salinity and temperature versus density

(Fig. 14). The differences between these three closures are that the first has the highest water level, and the second and third closures never get to the same level.

It is known that the first breach of the bar was artificial (Williams, 2014), openings that according to Behrens et al. (2013) would be less effective in keeping the mouth open than those that developed naturally, as in this case when the estuary is in an open state for just a couple days. The second barrier breach is believed to have occurred naturally.

In the time series, we observed during the closed state the temperature and salinity went stratified (Fig. 14). We observed a lower and non-stable temperature at the surface (Sensors 3 and 4 in Fig. 14) due to the cold season and the following day-night temperature changes. The temperature at the bottom (Sensors 1 and 2 in Fig. 14) is more stable, but still being influenced by daily changes and other external factors, indicating for example an abrupt fall on 13 Feb., followed by another increase. The bottom salinity is also steady most of the time and is generally decreasing. The surface salinity is more vulnerable to external factors and only is more stable during the closed state.

During the closed state, we observed three layers in the density structure with the superior one getting thicker upstream. In Fig. 16 there is the longitudinal view of the estuary densities from the profiles and the moorings. We can observe that near the mouth the salinity is higher or the water column is more homogeneous. After a few days in a closed state, the estuary opened on 12 Feb. and 3 Mar. observing a decrease in water level (Fig. 14).

### 5.1.3 Tidal and waves conditions

In Fig. 17 we have the wave conditions for Pescadero during the study period. We can observe, that when the mouth is open tidal influence is present in Pescadero, but when the mouth closes we cannot observe an evident effect in plain sight, which does not mean there is not present. Significant wave height goes from 2.5 m to more than 5 m approximately, but we have to account that deep water wave heights are larger than wave heights experienced at the coast (Williams, 2014), and as this data were collected 40 km from shore, thus we use this value as a proxy for coastal ocean conditions.

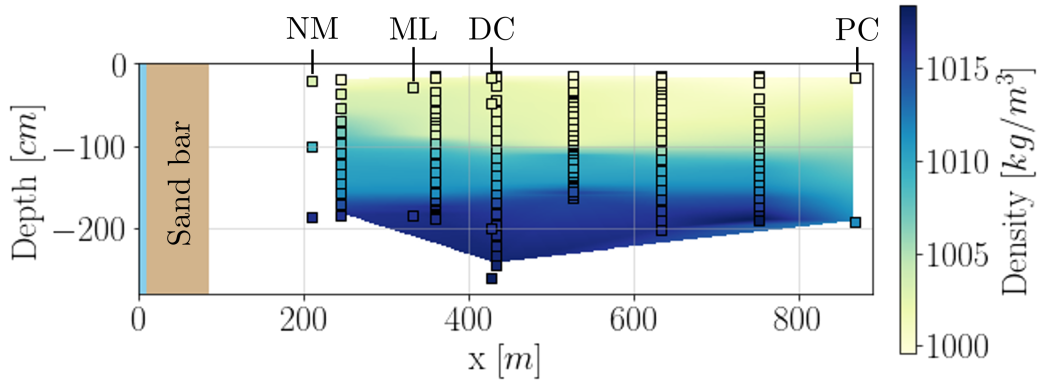


Figure 16: Along-estuary density colormap of Pescadero. Distance  $x$  is considered from the coast following the curvature of the estuary as the sensors are placed in Fig. 2.

The rest of the parameters (wave periods and direction) were collected from the same buoy, so they also are an approximation of the wave conditions. Dominant periods go from 5 to 20 s, while averaged periods have a range only between 7 and 10 s. The direction of the dominant period is stable at around 300 degrees most of the time, with just a peak on 29 Feb. where reaches 250 degrees.

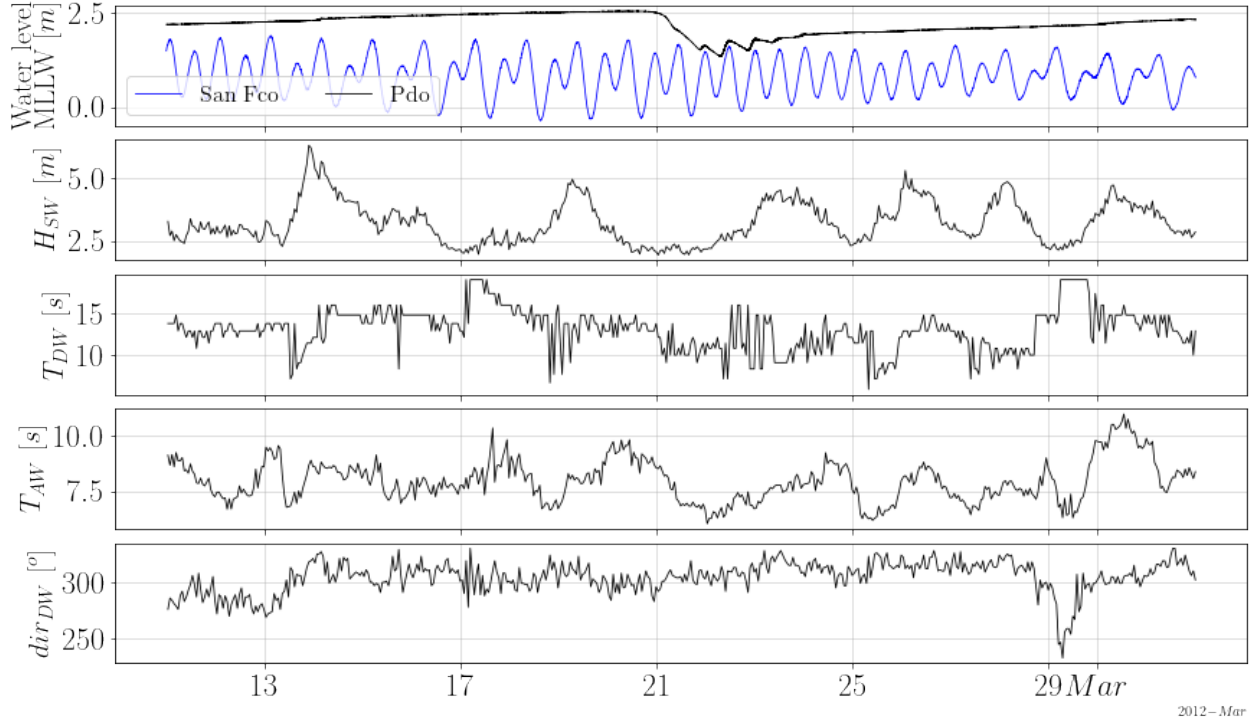


Figure 17: Time-series of tidal height in San Francisco (blue) and Pescadero estuary water level (black) in MLLW datum, significant wave height ( $H_{SW}$ ), dominant wave period ( $T_{DW}$ ), average wave period ( $T_{AW}$ ), and the direction from which the waves at the dominant period are coming ( $dir_{DW}$ ).

### 5.1.4 Pescadero creek discharge

Pescadero estuary receives freshwater from Butano Creek and Pescadero Creek, where the latter is the one that contributes the most to the lagoon and the one we have available data. When the inlet is closed, the maximum flow recorded was  $0.72 \text{ m}^3/\text{s}$ , lower than the usual for winters in California, presenting two small increases in flow (Fig. 18), but which, due to their low magnitude, would not be a determining factor in the rupture, considering that between July 2011 and July 2012 the maximum flow was  $29.73 \text{ m}^3/\text{s}$ . Even so, there is a constant inflow of fresh water that increase the estuary water level progressively until the inlet breaks.

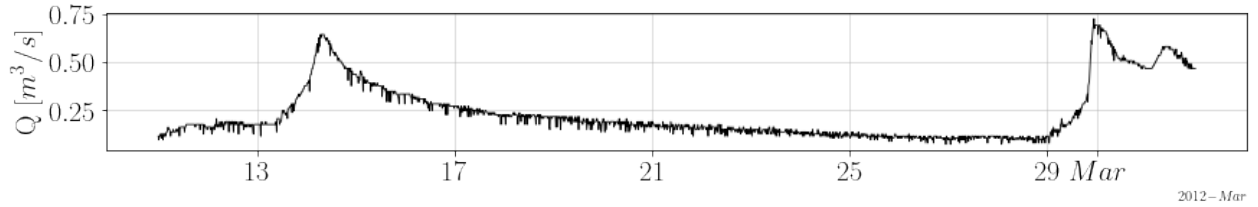


Figure 18: Time-series of freshwater flow from Pescadero Creek.

### 5.1.5 Currents speed and direction

During the closed state, the wind direction is predominantly onshore and its magnitude in that direction is bigger than in the rest of the period (See Fig. 12). Surface wind stress over the closed estuary causes the upper layer to go in the same direction as the wind, and the lower layer to move in the opposite direction (Katopodes, 2019). Given the limitations of the ADCP sensor, velocities near the surface were not always captured, therefore, there is a range of speed observable, not showing what happens at the bottom or the surface. Pescadero has its main directions very marked, a case that is very particular in this kind of estuaries, where along-estuary velocities always domain the currents.

### 5.1.6 Surface fluctuations

We can observe, that when the mouth is open tidal influence is present in Pescadero's water level, and when significant wave height increases the influence is also larger (Fig. 17). When the bar blocks the inlet, this causes accumulation of the upstream freshwater in the lagoon which is represented as an increase in Pescadero's water level. The closure reduces the ocean influence to be negligible to plain sight, but still could be wave overtopping the inlet sandbar. These wave overtopping events could be detected by the fluctuations in the surface present in the data, but also we have to consider the fluctuations caused by wind stress or by an increment of the discharge.

## 5.2 Hydrodynamic controllers

The external factors that could be affecting the estuary in a closed state are freshwater inflow, saltwater overtopping from waves, and wind stress. There are other factors involved as temperature or evaporation, but we estimated that those were negligible due to the haline stratification that dominates the estuarine structure.

### 5.2.1 Stratification controllers

At the beginning of both periods of disconnection, we noticed that there were changes in densities on the surface and in the deep layer, although the latter in smaller magnitude and fewer times (Fig. 19). Three important wind events occurred in each period that matches with the increase in surface densities, observing that when the stress on the surface increases, so does the density in the upper layer in the three sites. When wind forcing decreases, we noticed that density tends to return to its initial state, except for the largest events at the beginning of each period, where density at the bottom is smaller after the event than before.

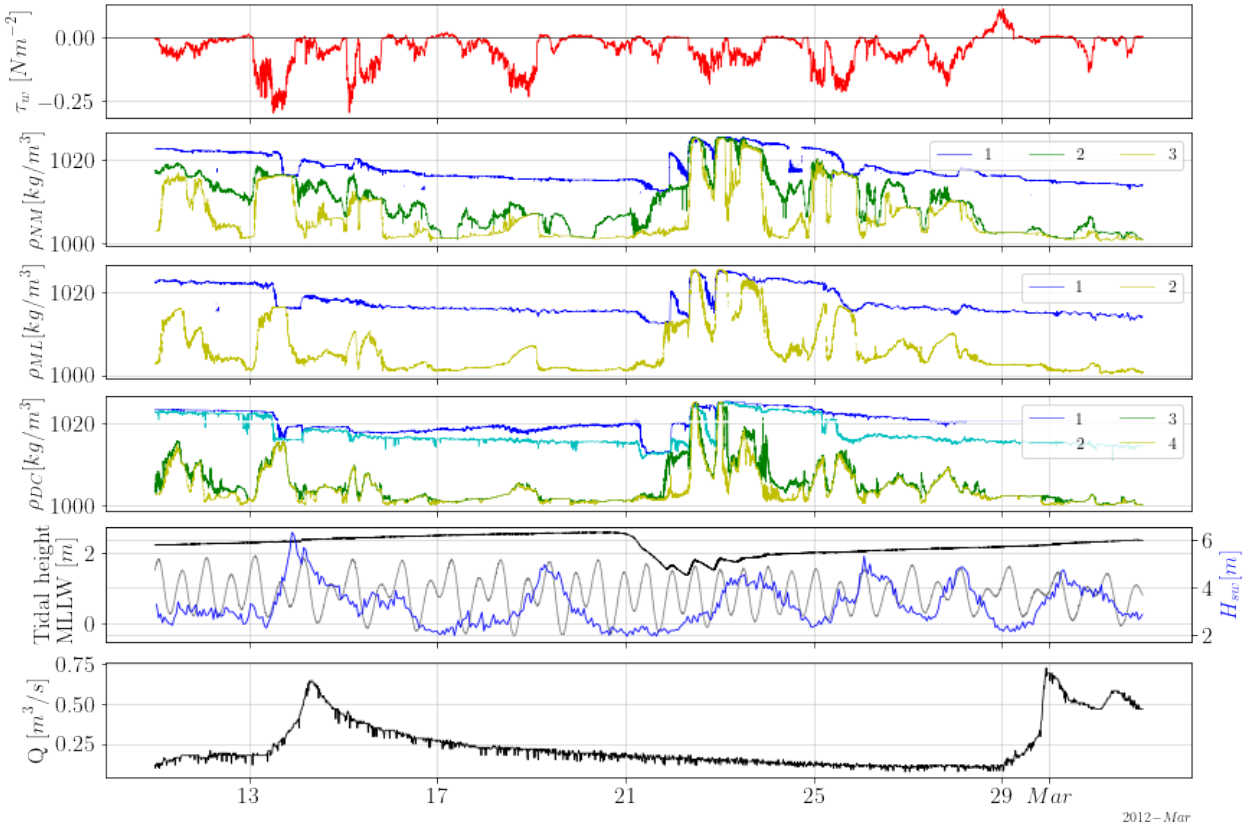


Figure 19: Time-series of wind stress ( $\tau_w$ ), NM ( $\rho_{NM}$ ), ML ( $\rho_{ML}$ ), and DC ( $\rho_{DC}$ ) densities in different depths, where sensor 1 is the deepest and sensor 4 is the shallowest (The positions in the water column of the sensors are shown in Fig. 16), significant wave height in Halfmoon Bay in blue ( $H_{sw}$ ), Pescadero estuary water level (black) and tidal height in San Francisco (gray) in MLLW datum, and freshwater inflow of Pescadero creek ( $Q$ ).

Upstream inflow had two increasing events in the studied period (Fig. 19) and during those events, there wasn't an instant change in density, but we could notice a trend in density, especially in the lower layers, which was decreasing in time during both disconnected periods on NM and ML sites. In the first period, at the DC location, unlike the others, there was an increasing trend of density, which would not be unusual considering the lower layer of DC is much deeper than the ones of NM and ML (Fig. 16), furthermore, the layer in DC with the same depth to those is the one before the deeper (in cyan, Fig. 19). Another change in density that is noticeable occurs in the middle layer of NM (in green, Fig. 19) between 13 Feb. and 17 Feb., just before and after there was an increase in discharge. There we observed that density went from around

$1015 \text{ kg/m}^3$  to almost  $1000 \text{ kg/m}^3$ .

Significant wave height and tidal height could be showing some wave overtopping events when there is high tide and high waves, but this does not mean there couldn't be wave overtopping when there is only high tide. Even though we do not observe important increases in density that indicate an important saltwater input, so we cannot know when happens. Anyways, there are small changes in density both on the bottom and on the surface.

First, we observed density fluctuations at the surface but without causing important changes on 14 Feb., 16 Feb., 19 Feb., 20 Feb., 26 Feb., 27 Feb., and 1 Mar, while there was high tide and sometimes high waves, but all of them happened right after a wind event or during an increase of discharge (Fig. 19), so we can't assume that one factor or another is causing it. Second, at the bottom, we observed some density increases that were momentary on 15 Feb., 26 Feb., 27 Feb. and 28 Feb. during high tide, and mainly noticeable in NM, which is the closest site to the sea. Those increases do not look like the increases in salinity caused by wind effects, because the salinity is bigger than before the wind event in some cases, although, as this still happens when there was a wind event we can't attribute it just to wave overtopping. Third, there was a continuous increase in DC at the bottom that happened after an important decrease in salinity due to a wind event.

### 5.2.2 Surface fluctuations controllers

If we focus on the depth at Pescadero we can observe more clearly how external factors are changing the estuary. The wavelet frequency analysis of depth can show the effects of the waves into the lagoon, by identifying changes in its fluctuations and showing when there is the presence of certain frequencies that could represent the ocean influence. If we crossed this information with tidal behavior and significant wave height we can obtain a more certain way to identify wave overtopping events.

We notice that when the estuary is open the ocean effects are very marked in the wavelet analysis (Fig. 20). During a closed state, the effects are also evident but more slightly, with more concentrations of frequencies between 0.02 and 0.1 Hz, and we could point out that those are wave overtopping events. Also, we can say that they occur exclusively at high tide, and any wave height, but the events are bigger when the waves are larger. On the other hand, wave overtopping does not have a clear pattern of behavior in  $dh/dt$  or  $(\hat{H}_{DC} - \hat{H}_{ML})/\Delta x$  when the inlet is closed.

As we notice earlier, the discharge has two increase events during the studied period. We can observe that those increases are affecting directly the surface, showing important peaks of  $dh/dt$  during those events (Fig. 20). Also, the change of the standardized height in the horizontal ( $\Delta\hat{H}/\Delta x$ ) showed at the beginning of the period negative values which changed to positive values after the increase of discharge, which also results in happens after a strong wind event and during a wave overtopping.

## 5.3 Wind-driven effects

As mentioned before, we noticed changes in density at the same time there were wind events, therefore for quantifying those changes we calculated the potential energy anomaly of the water column in location NM and compared it to wind stress (Fig. 21), where we noticed that there were a lot of similarities between both time-series. We observed that when wind stress magnitude increases, potential energy anomaly decreases,

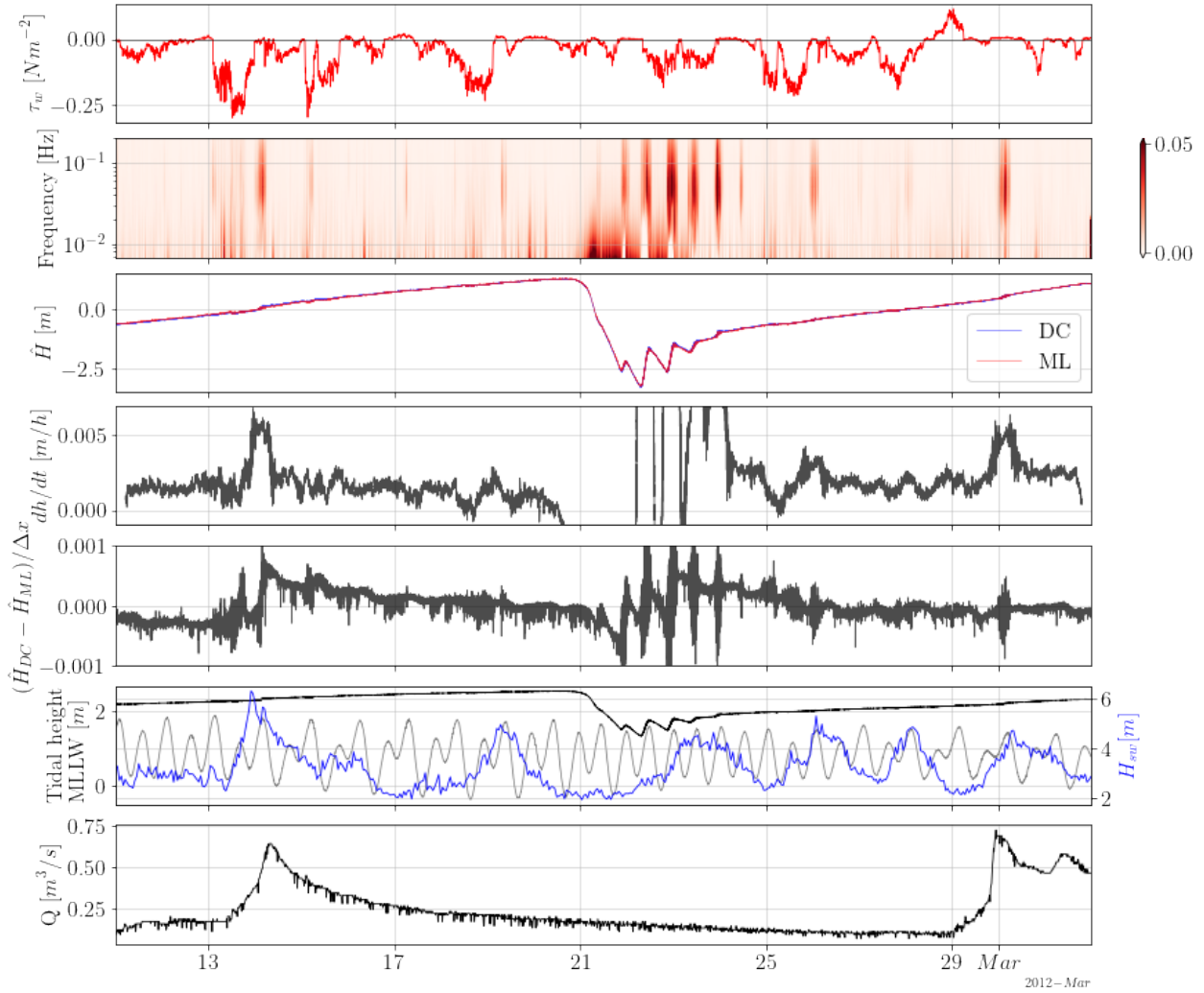


Figure 20: Time-series of wind stress ( $\tau_w$ ), depth wavelet frequency analysis at DC, standardized depth ( $\hat{H}$ ) in DC, NM, and ML locations, the change of the water level in a 10-hour frame ( $dh/dt$ ), standardized depth change between locations DC and ML ( $(\hat{H}_{DC} - \hat{H}_{ML})/\Delta x$ ), significant wave height in Halfmoon Bay (blue), Pescadero estuary water level (black) and tidal height in San Francisco (gray) in MLLW datum, and freshwater inflow of Pescadero creek ( $Q$ ).

except when there are positive values like on 28 Feb. and 29 Feb, when there was no change in potential energy anomaly. However, we can notice that the potential energy anomaly has not the same behavior in wind events of the same magnitude, and we can observe that, in time, wind decreases its effect on the potential energy anomaly, only reaching 0 at the first wind event of each period. In addition, we can observe that after those events there is a decrease in potential energy anomaly when wind stress is zero, probably showing a change in their stratification structure after those events.

For further understanding, we implemented the Wedderburn number to observe if there was upwelling due to wind events. As we did not have the thickness of the epilimnion we estimated a range of positions for the pycnocline. This range started right after the first CTD, the deeper one (in black), and ended in the second

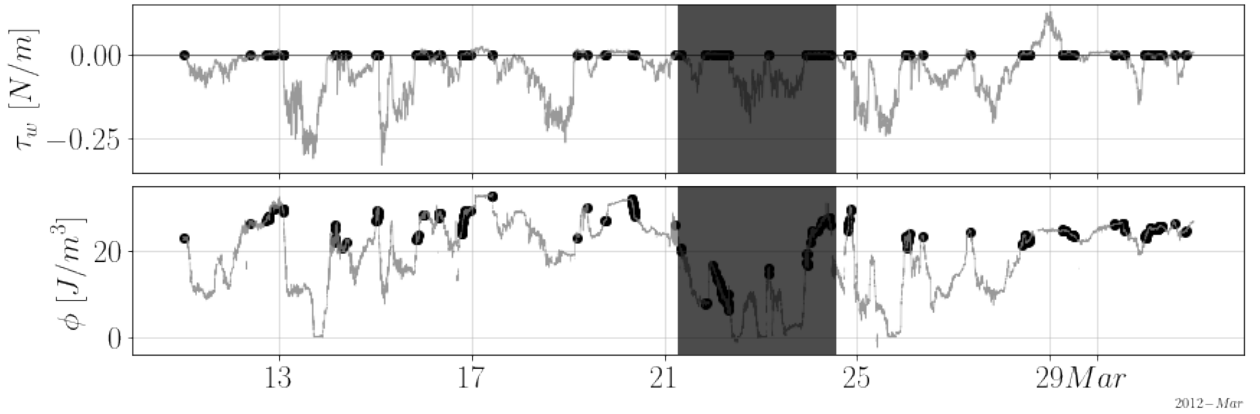


Figure 21: Time-series of wind stress ( $\tau_w$ ), and potential energy anomaly ( $\phi$ ). Dots are the instant when wind stress is zero. The shadowed window is when the estuary is in an open state.

CTD (in grey) (Fig. 22). Also, we marked with a star where was the epilimnion limit on 16 Feb., when we had more information on the density (Fig. 16), which could be changing in time. As we are working with a range of values, we considered a partial upwelling when just the upper boundary reaches  $W=1$  and full upwelling when both boundaries reach that value. In each period we noticed one full upwelling event and two partial upwelling events, for a total of six upwelling events observed in the studied period, always the first one being fully upwelled (Fig. 22). After full upwelling events, density at the bottom of the water column did not come back to its original values from before the event.

In Fig. 23 we can observe how density at the surface is getting more resilient to wind effects over time. The three wind events in the first period are similar in magnitude, but the increase in density that they trigger is each time smaller. What's more, we can notice a small wind stress event at the beginning of the time series that increased density three times more than the last wind event in the period. We can also notice that density changes in the vertical ( $\Delta\rho/\Delta z$ ) reached 0 at the first wind event of each period, but then, after the event,  $\Delta\rho/\Delta z$  went steadier and didn't reach 0 again during the period.

The first important wind event started on 13 Feb. at 2 a.m. and the first location that was affected was NM, then ML, and finally DC. We can prove the latter with the change of density along the estuary (Fig. 23) where we observed negative values almost all the time, showing higher values in NM than in DC. When the wind starts to blow there is an increase in  $\Delta\rho/\Delta x$  magnitude, and after reaching the peak the value decreases again to zero and stays there if the wind speed is constant. If wind speed decreases there is another increase in  $\Delta\rho/\Delta x$  magnitude, showing that the wind stops influencing DC location first and then NM.

To quantify the time difference between the moment the wind started blowing and the density started changing at the different CTD locations, we calculate by visual inspection how long it took for the wind to affect density at different points. To achieve this, we considered the moment that density just started to change into a trend after the wind started or stopped blowing. Also, to compare the obtained values we calculated the cross-correlation, between density and wind stress, after normalizing and standardizing both signals. We obtained the values of the first wind event, and how long took to start and finish, and for the cross-correlation, we added the total of the first-period lag.

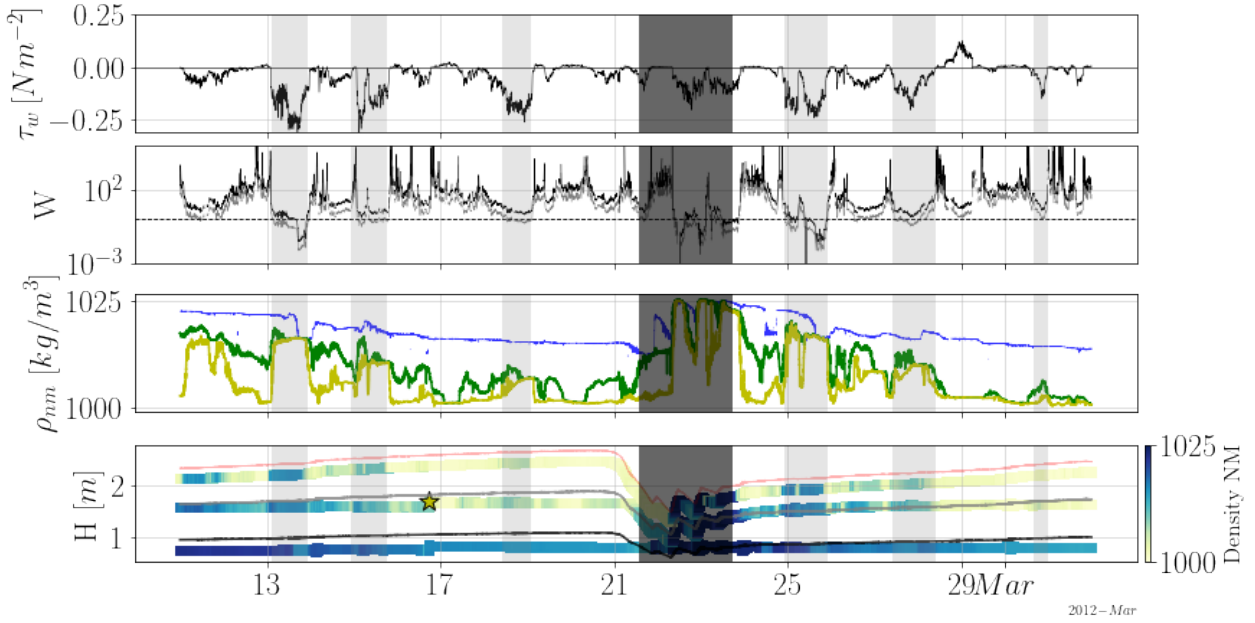


Figure 22: Time-series of wind surface shear stress ( $\tau_w$ ), Wedderburn number ( $W$ ) where the dashed line shows  $W=1$  and black and gray lines show  $W$  obtained at the lower and upper part of the selected window respectively, density at the bottom (blue), middle (green), and top (yellow) of the water column in NM location ( $\rho_{nm}$ ) (see Fig. 16 for sensors positions), and colormap of density in time-space at each sensor of location NM with the black and gray line that limit the lower and upper part of the window of possible values for top layer width. The dark shadowed window is when the estuary is in the open state. Light-shadowed windows are when the upwelling events were observed. Redline is the water level, and the star indicates where the surface layer ends according to Fig. 16.

In Table 2 we observed that surface sensors (NM3, DC4, and ML2) had no delay with the cross-correlation method and did have it in the visual inspection. Also, with the latter method, we observed that NM3 was the last sensor that started to change after wind stress started, but it increased faster than the others, a fact that we can observe slightly in Fig. 23 for  $\rho_{top}$ . Also, we observed that the one that took longer to come back to its initial value was NM3, then ML2 and DC4.

If we compared Table 2 values to the response tilt time, obtained as the fourth part of the internal wave period, that is  $11.75 \pm 2.72$  min, we observe that it is the most approximate to the values of the total period obtained by cross-correlation at the surface, but they are the double of it. Also, at the beginning of the event by visual inspection DC4 takes 10 minutes to start changing which, considering that DC is at the center of the estuary, could be the correct value.

Surface wind stress over the closed estuary causes the upper layer to go in the same direction as the wind, and the lower layer to move in the opposite direction (Katopodes, 2019). Given the limitations of the ADCP sensor, velocities near the surface were not always captured, therefore, we observed a range of speed, not showing what happens at the bottom or the surface. On the other hand, Fig. 24 shows that the along-estuary speeds ( $u$ ) increase in proportion to the wind stress, but in opposite direction. The wind is also influencing cross-estuary velocity ( $v$ ), but with less intensity due to the wind's main velocities. Vertical velocity ( $w$ )

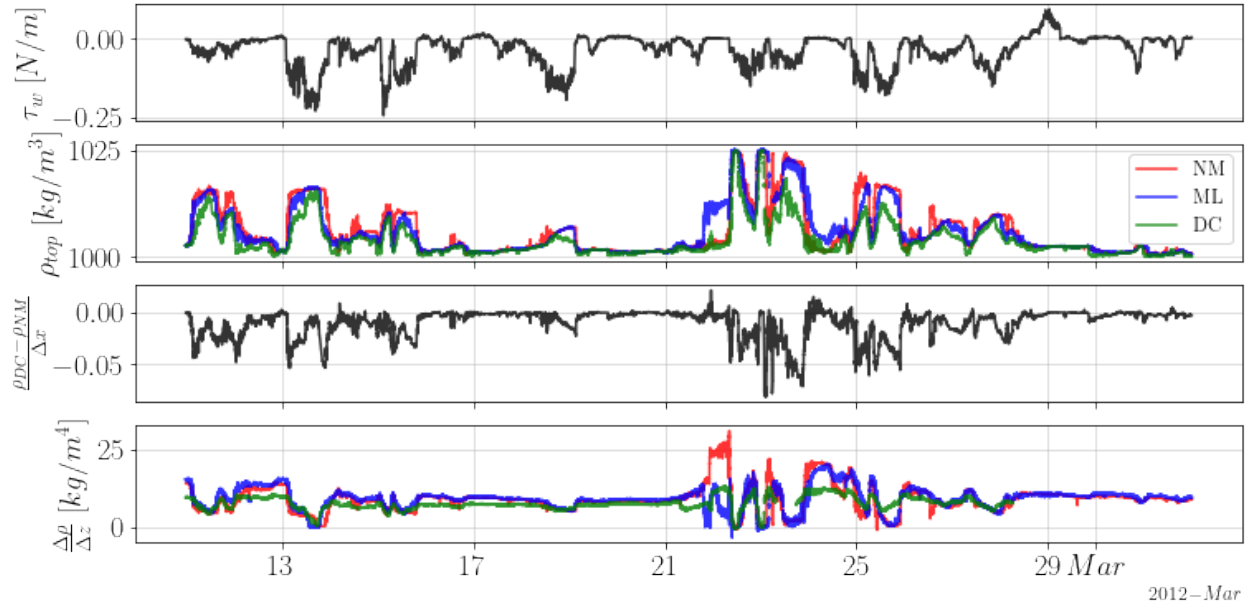


Figure 23: Time-series of wind shear stress at the surface ( $\tau_w$ ), surface densities in locations NM, ML, and DC ( $\rho_{top}$ ), density change between locations DC and NM at the surface ( $\frac{\rho_{DC} - \rho_{NM}}{\Delta x}$ ), and density change between surface and bottom in locations NM, ML, and DC ( $\frac{\Delta \rho}{\Delta z}$  [ $\text{kg}/\text{m}^4$ ]).

presents fluctuations and some negative or positive peaks during wind events or after in some cases.

The observed dynamic of the upper velocity at the window shown in Fig. 24 is such that when wind stress has positive velocity, considering positive the direction of the streamflow, the along-estuary water velocity is negative and vice versa. The magnitude of wind stress does not change this behavior along time, but as the water level increase, the estuarine velocity gets smaller for the same wind-stress magnitude. However, when wind stress is very small the dynamic change, and the upper along-estuary velocity at the window goes in the same direction as the wind stress at the surface.

Table 2: Lag obtained by cross-correlation method and visual inspection. "Start" columns mean that lag was calculated only when the wind stress magnitude was increasing at the first event, and "end" columns mean that lag was obtained when the wind stress magnitude was decreasing at the first event.

Method	Cross-correlation				Visual inspection		
	Sensor	Start	End	Total event	Total period	Start	End
NM1	252 min	132 min	354 min	384 min	810 min	420 min	615 min
NM3	0 min	0 min	0 min	36 min	30 min	225 min	127 min
DC1	36 min	0 min	258 min	732 min	630 min	30 min	330 min
DC4	0 min	0 min	0 min	30 min	10 min	0 min	5 min
ML1	54 min	174 min	450 min	600 min	615 min	500 min	557 min
ML2	0 min	0 min	0 min	24 min	0 min	55 min	27 min

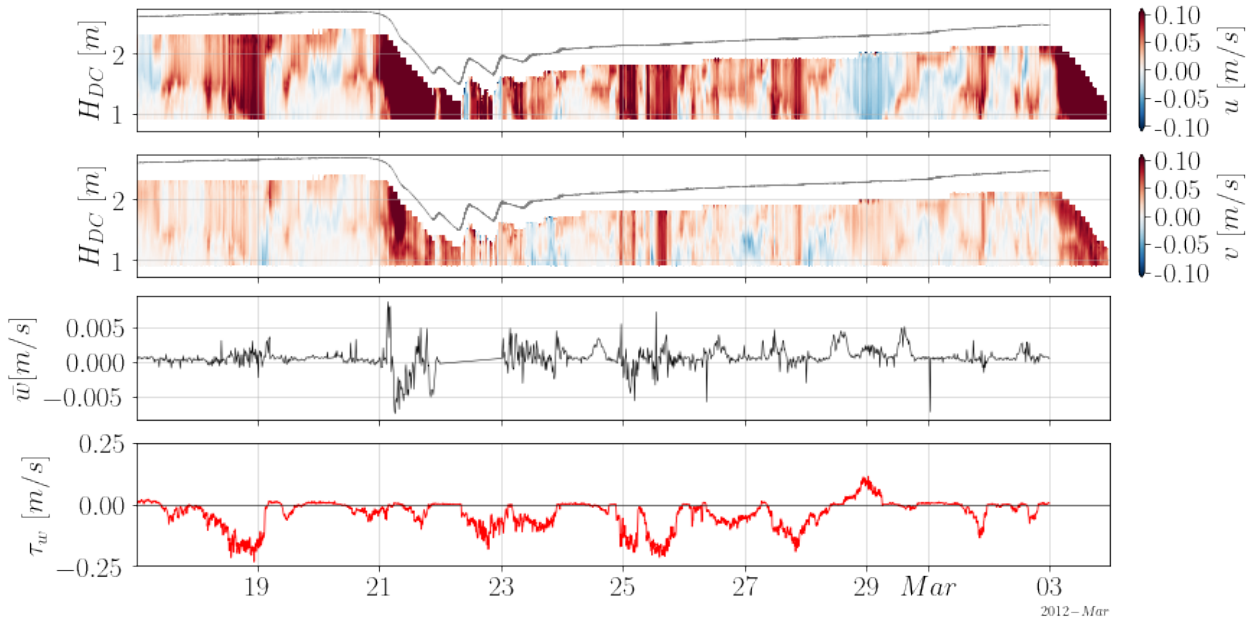


Figure 24: Time-series of:  $u$  and  $v$  in the vertical, averaged vertical velocity, and wind stress.

For the average vertical velocity in the water column ( $\hat{w}$ ) (Fig. 24) we can observe mainly positive values (upwards), but there is no interesting behavior in it until the second period when we observed more changes, other than small fluctuations during a wind event. We could observe important peaks when the wind was starting to blow and, in some cases, right after the wind finished, showing that layers are going upwards at that moment. Also, we observed negative values during the first wind event on the second period, showing probably that the surface tilt is returning to its initial state.

To observe in detail the behavior of the water column, densities and velocity profiles for each sensor were plotted in certain instants in the first wind event of the second period (Fig. 25). This wind event is characterized by two wind increases and a period in the middle with small wind stress that lasted 3 hours approximately. The profiles before the event, during the first increase, the middle period, the second increase, and after the event were plotted.

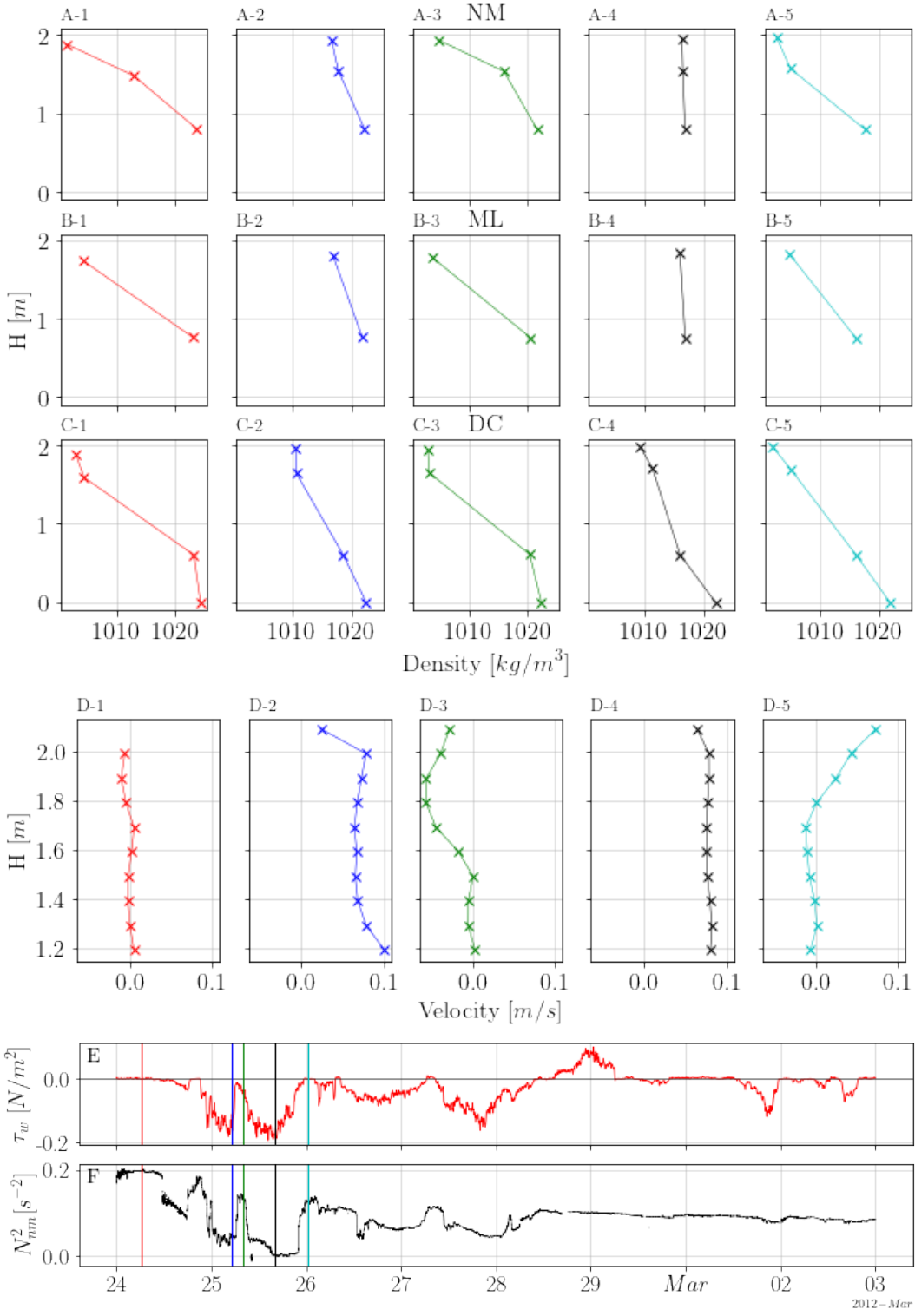


Figure 25: Density profiles at locations (A) NM, (B) ML and (C) DC, and (D) velocity profiles of 5 moments before, during, and after a full upwelling event, and time-series of (E) wind stress and (F) buoyancy frequency showing the plotted instants.

We could notice that before the wind event the water column is stratified, and the velocity is zero. During the first part of the event, the principal effect is the density increase near the surface and the positive velocity in all the visible part of the water column. Then, when the wind stopped the estuary went stratified with similar values of density to the first profiles, but the velocity had a different behavior, and went negative in the upper layer, probably showing that the water is returning to its original state or that when wind stress is too small the surface water that goes into the same direction of the wind gets thicker and starts to be detected by the ADCP. When the wind reaches its maximum the water column is less stratified than in the first increase and velocity has bigger values. Finally, the last profiles show positive velocities at the surface and as there is no wind at that moment, maybe is showing the freshwater passing through the estuary, also, the density profiles show a stratified estuary but less than before the event, meaning there was mixing in the water column during the wind event.

When the wind is blowing inland, shear stress causes a set up at the end of the estuary by driving water away from the free surface, increasing upstream hydrostatic pressure and causing estuarine recirculation. This causes the pycnocline to move towards the surface and increase in density where the surface layer used to be. This is what is happening in Fig. 25, where NM has been affected first and more abruptly than ML and DC, the latter being the one that changes its density the least. This may be because NM is the closest sensor to the mouth of the estuary, and therefore it is the one that detects the pycnocline first, followed by ML and DC.

On the other hand, buoyancy frequency values when wind stress is zero decreased, going from 0.2 to 0.1  $kg/m^3$  showing less stratification after the big wind event. Also, we can notice that  $N^2$  is steadier after the wind event and decrease less for winds of the same magnitude (Fig. 25).

In Fig. 26 there is a closer look of the surface fluctuations behavior. First, in the wavelet analysis we observed three events of wave overtopping, which show a concentration of frequencies in the range from  $2 * 10^{-2}$  to  $2 * 10^{-1}$  Hz. Also, we observed that during the wind event the frequencies showed less concentration than in the wave overtopping event and was observed in the range of frequencies between  $10^{-2}$  and  $2 * 10^{-1}$  Hz. Second, the standardized height ( $\hat{H}$ ) showed an increase with a positive peak when the wind started blowing, which when it went stronger decreased to negative values with lots of surface fluctuations. When the wind stopped the height return to positive values near 0. This is indicating an inclination of the surface or a set up.

The change of the depth in time showed mainly positive values almost all the period (Fig. 26), meaning that the water level is increasing most of the time. The only moment when the change was negative for more than an hour occur at the beginning of the wind event. Also, at the end of the time series there is a peak of negative values with unknown cause. The difference between the standardized height of DC and ML along-estuary indicates that when this value increases, the height in ML is smaller and the height in DC is larger, and vice versa. This could be caused by both the wind and other external factors such as inflow from upstream, flow that may be entering or escaping through the sand bar, among others. In Fig. 26 at the beginning of the time series the values of  $\Delta\hat{H}/\Delta x$  are oscillating slightly around 0 with a wavelength of 24 h approximately. When the wind started blowing, the values turned negative, showing that DC decreased more than ML. After the wind event, the values continued the oscillations, but with more amplitude than before.

The spectral analysis of the depth in DC, ML and NM shows that between frequencies of  $4 * 10^{-3}$  and  $1 * 10^{-2}$  Hz, around a period of 2 min, there is an increase in Power Spectral Density (PSD) (Fig. 27), showing us the presence of infragravity waves in Pescadero. If we add to the spectral analysis the wind stress and compare it we observed some similarities in the frequencies. Between  $8 * 10^{-5}$  and  $1 * 10^{-4}$  Hz there is an increase in PSD for wind and depth at NM, that is for the period around 200 min, and also between  $1 * 10^{-4}$  and

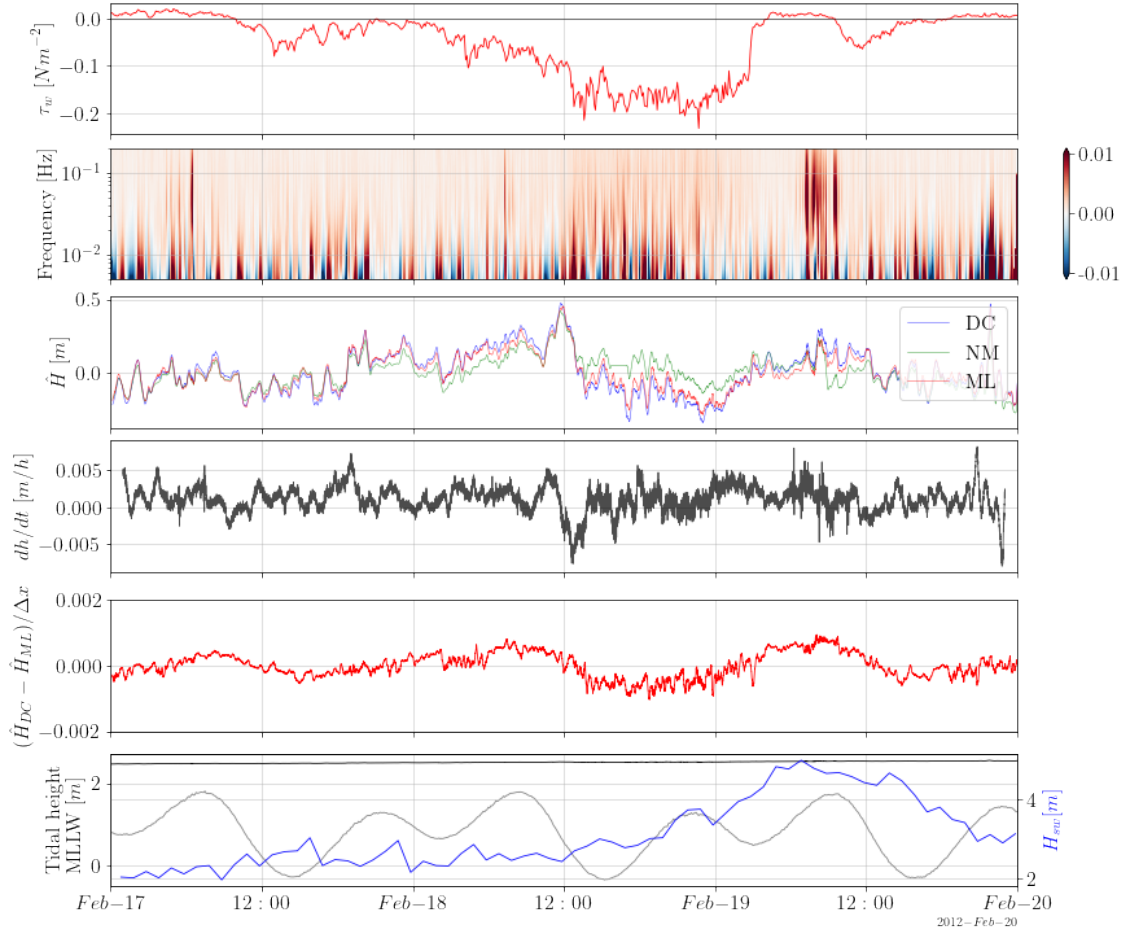


Figure 26: Time-series of wind stress ( $\tau_w$ ), depth wavelet frequency analysis at DC, standardized depth ( $\hat{H}$ ) in DC and ML locations, the change of the water level in a 2-hour frame ( $dh/dt$ ), standardized depth change between locations DC and ML ( $(\hat{H}_{DC} - \hat{H}_{ML})/\Delta x$ ) with its rolling mean, and significant wave height in Halfmoon Bay (blue), Pescadero estuary water level (black) and tidal height in San Francisco (gray) in MLLW datum.

$1.1 * 10^{-4}$  Hz we notice peaks in wind and depth in ML and DC, that correspond to 140 min approximately. In addition we observed two peaks in wind stress between  $2 * 10^{-5}$  and  $5 * 10^{-5}$  Hz, that is between 700 and 300 min, while in the depth spectrum we observed some increases in the three sites for the same range but with less significance.

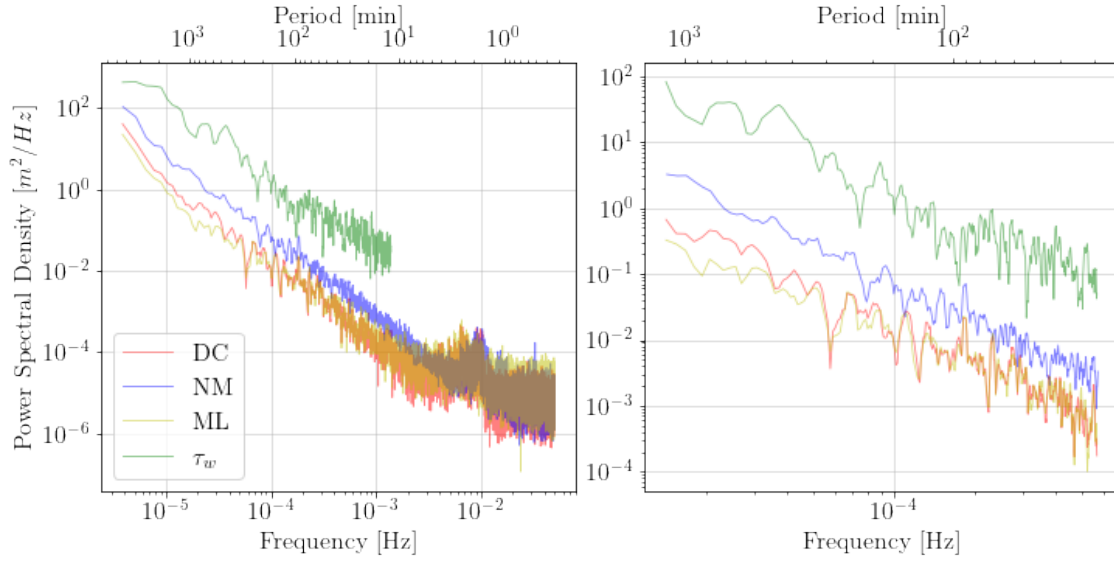


Figure 27: Frequency spectra of water level fluctuations in the estuary at sites in NM, DC and ML, and of wind surface stress between 11 Feb. and 20 Feb. with a close up of the lower frequencies.

## 6 Discussion

When the mouth of an estuary is closed, it can become vertically stratified due to the freshwater input and the occasional wave overtopping of saline water. In such circumstances, it becomes difficult to energize the water column. However, external factors such as wind stress on the surface, discharge and wave overtopping can cause vertical transport in the water column (Roberts et al., 2021). In the case of Pescadero, vertical transport could not be driven by density exchange, as the estuary would always be saltier than the input water from the creeks, resulting in a consistently stratified water column. Nevertheless, there exists a light density/salinity gradient in Pescadero due to the freshwater input from upstream and saltwater overtopping the bar at the other end.

### 6.1 Estuarine structure and morphology

During the winter of 2012 Pescadero estuary received less fresh water inflow compared to other months throughout the year, leading the inlet to disconnect from the ocean. Pescadero during its closed state function as a stratified coastal lagoon with river runoff forming a surface layer of fresh water and occasionally having tidal inflows of saline water. The orientation of the bay and the shallowness result in the exposure of all the water columns to the wind stress events. In this regard, Pescadero shares many physical traits with other bar-built estuaries where the local wind forcing is the dominant driver.

Apart from the stratification, there is an along-estuary density gradient between the outlet of the creek and the mouth, due to the constant discharge of freshwater. Near the mouth, the upper layer is thinner than in the creek's outlet, probably because the salinity is higher in the mouth due to the waves that are overtopping the sandbar along with upstream continuous freshwater input.

The present study analysis reported that the major driver of mixing is wind stress and the major driver of water level variability is freshwater inflow, even in periods when it is very low. In the next sections, we are going to

discuss the role of other factors that affect Pescadero and its importance in stratification and water level.

## 6.2 Analysis methods

Wind and estuarine velocities were axis-rotated in the direction of maximum variance of water currents (See Fig. 7, Section 4.3.2), but there was also the option of doing it in the direction of wind velocity. This puts the main focus on the estuary currents instead of the wind velocity, but in this particular case, both, wind and water velocities, have a similar principal direction, so it wouldn't be a big difference between each option.

We adjusted the first cell of the ADCP data by visual inspection, using the blank space given by the ADCP, which was 0.71 m, and overlapping it with the CTD data on the same location DC. This comparison gave us the value of 0.91 m for the first cell location, which is merely an estimation, so it could have been a different value, bigger or smaller depending on how we had placed the overlapping. This does not affect velocity values, but we have to consider it for the positions of the layers or the profiles, but it does not make an important change in the analysis.

The closed state definition was set in a range of depth's change in time values with a 10-hour frame. The frame was selected by trial and error based on the timescale we were working on and it could change depending on the period in which the data was collected and the data collection frequency. Also, we have to consider that the opening and closures do not happen in an instant, but in a process that could last from minutes to hours, so it could be considered any instant during that process. In this case, the registered openings lasted 4, 21 and 28 hours each.

In this study, we did not consider temperature and evaporation factors. We considered that the effect of temperature was not important due to the haline stratification that dominated the estuary, but it could be studied in greater depth in future analyzes in Pescadero. Also, we didn't consider evaporation as a factor for depth changes because we are studying an estuary with a small area, and as it was winter time the air temperature was not too high to cause major impacts.

To calculate wind stress we used a drag coefficient defined by Large and Pond (1981), but according to Paugam et al. (2021) the drag coefficient  $C_D$  can be difficult to estimate in shallow water, so we have to consider the obtained  $C_D$  as an approximation in the wind stress and everything calculated with that coefficient. In future studies, there could be used other drag coefficients to observe if there is a big difference in the wind stress and other indices obtained with  $C_D$ .

The Wedderburn number was obtained with the equation for a rectangular basin defined by Monismith (1985), so it is showing us an approximated value. Despite this, it is still a good indicator to estimate the behavior of the stratification to wind stress. We could try in future research more adapted Wedderburn numbers to the Pescadero basin and compare the results with those obtained in this study.

The frequency spectral analysis only shows a general view of the most important frequencies in the dataset but does not show the specific time when this happens. This makes it a special tool to detect frequency peaks and contrasting different datasets.

### 6.3 Wind stress mixing

Strong wind events were an important part of estuarine dynamics in Pescadero, inducing changes in circulation and stratification. Between November and January, sporadic strong wind events were recorded, with 3 to 4 events per month. However, during the study period, an increase in the occurrence of these wind events was observed, reaching between 7 and 8 events per month 28.

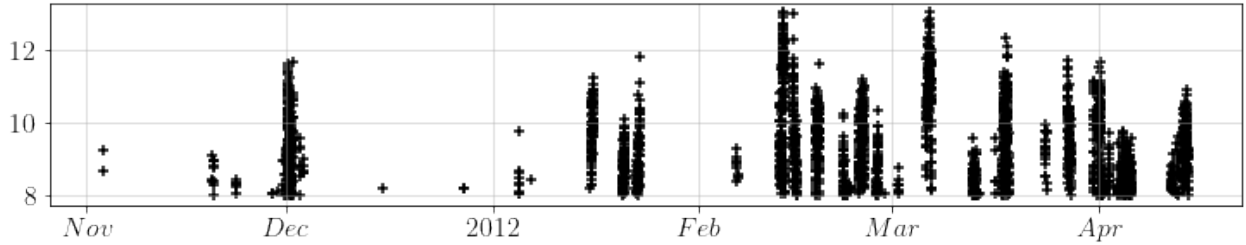


Figure 28: Occurrence of strong wind events in Pescadero estuary.

Sporadic abrupt changes in density along the water column in different locations were apparent during the periods of the closed state. These sudden changes indicate that they were not caused by gradual processes, but rather resulted from sporadic events that are attributed to the effects of wind stress present at the same time as the density changes. After these events, density did not return to its original values from before the event so mixing was present in the three studied locations.

Fig. 25 is showing density profiles in the studied locations before (in red) and after (in cyan) a big wind event, showing a difference in the density values, especially in the bottom where there is a decrease in density. Buoyancy frequency showed a decrease after the wind event meaning a change in stratification, same as the potential energy anomaly in Fig. 21. Also in Fig. 23  $\Delta\rho/\Delta z$  is showing a decrease in stratification between before and after big wind events, only observing this abrupt change twice, with one time during each closed state period.

We chose to obtain a range of values for the Wedderburn number as we did not know the exact placement of the pycnocline. Due to the constant freshwater inflow, the stratification of the estuary is changing over time, which means the surface layer is also changing its thickness. The range limits of W were obtained as a function that depends directly on the water level. We assumed the density interface theoretically reaches the upwind surface at  $W = 1$ , so if the full range of W goes lower than that value we will consider it a full upwelling. During a full upwelling, if we consider a linear tilt, the lower limit reaches the surface, different from partial upwelling, where just the upper limit reaches the surface. The main difference between both events of upwelling is that the full one is changing the density structure and the other one is not. We can observe this in Fig. 21 where the potential energy anomaly after the partial upwelling events is not changing. During the upwelling events, there is the presence of baroclinic pressure gradients which increase with a lower W, so during the partial upwelling events, the gradients are not enough to mix the water column and change the stratification structure.

On the other hand, we observed surface fluctuations during the wind events, which are noticeable in the wavelet analysis in Fig. 26. Also, there is a small relation between wind and depth density frequencies (Fig. 27) around a period of 200 min.

## 6.4 Wind-driven circulation

During and after wind events there were observed circulation processes that are indicating how the layers of the estuary behave. We already noticed that the main driver of changes in velocity in the estuary is wind stress. In Fig. 29 we observed with more detail the circulation occurring around the first wind event of the second period. We observed that the estuary had some circulation occurring before the event, when there is no wind stress, due to the constant freshwater inflow that is present in Pescadero. This velocity is positive (streamflow direction) and is at the superior layer detected by the ADCP. Also, before the wind event, with  $\tau_w = 0$ , there was a negative velocity at the top of the range occurring at the same time as a detected wave overtopping event, meaning that the waves were creating a small circulation in the surface of the estuary that was overlapping the discharge velocity.

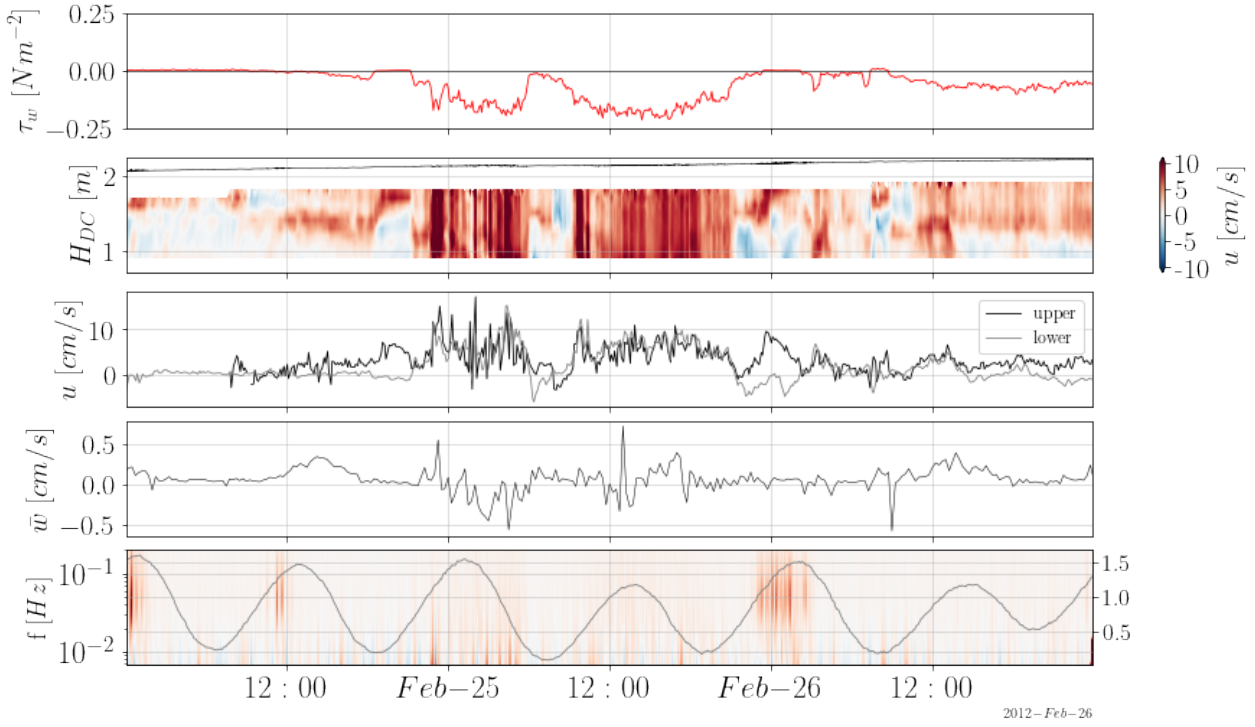


Figure 29: Time-series of wind stress ( $\tau_w$ ), along-estuary velocity in the water column, along-estuary velocity in the upper and lower layers of the ADCP range, and depth wavelet frequency analysis at DC and tidal height in San Francisco (gray).

During the wind event, we observed an increase in velocity in the positive direction, while the wind stress is negative. The literature says that a stratified waterbody that is subjected to surface stress has its surface layer circulating with the same direction of the wind with a set-up of the free surface at the leeward zone, depressing the pycnocline and resulting in set-down at the wind leeward shore and circulation of the lower layer in the opposite direction of the wind (Katopodes, 2019). Despite the last statement we observed in Fig. 29 the velocity during a wind event is in the opposite direction of the wind. This is due to the range of available data from the ADCP, which starts measuring at 0.91 m and doesn't work near the surface, not showing the surface layer circulation and skipping the part where the velocity is in the same direction as the wind. Also, when the wind blows, the upper layer moves towards the surface and upstream moving away

from the detected range (Fig. 30) making the upper layer thinner at the DC location.

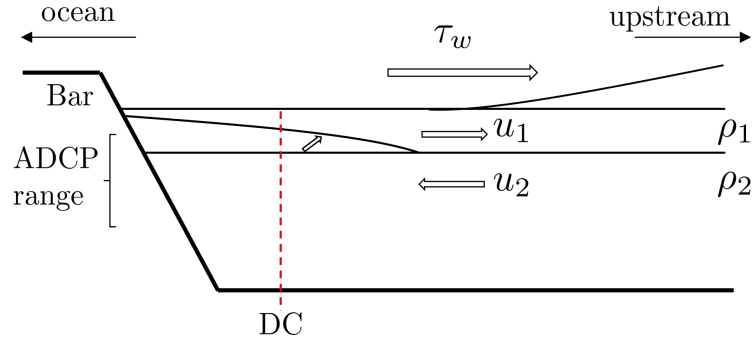


Figure 30: Scheme of the pycnocline tilt in an idealized estuary with the detected ADCP range in Pescadero.

Following the relaxation of the winds, the baroclinic pressure returns the estuary to its original state generating currents which are present mostly at the lower layers of the ADCP range (Fig. 29). We observed negative velocities after the first relaxation between the two wind increases. First, negative velocities were present at the lower part, representing the return of the middle layer to its equilibrium position, while at the top velocities were positive, maybe showing the surface layer dynamics. After less than two hours there was a flip on the dynamics, at the upper part positive and the lower negative, meaning probably a seiche in the estuary.

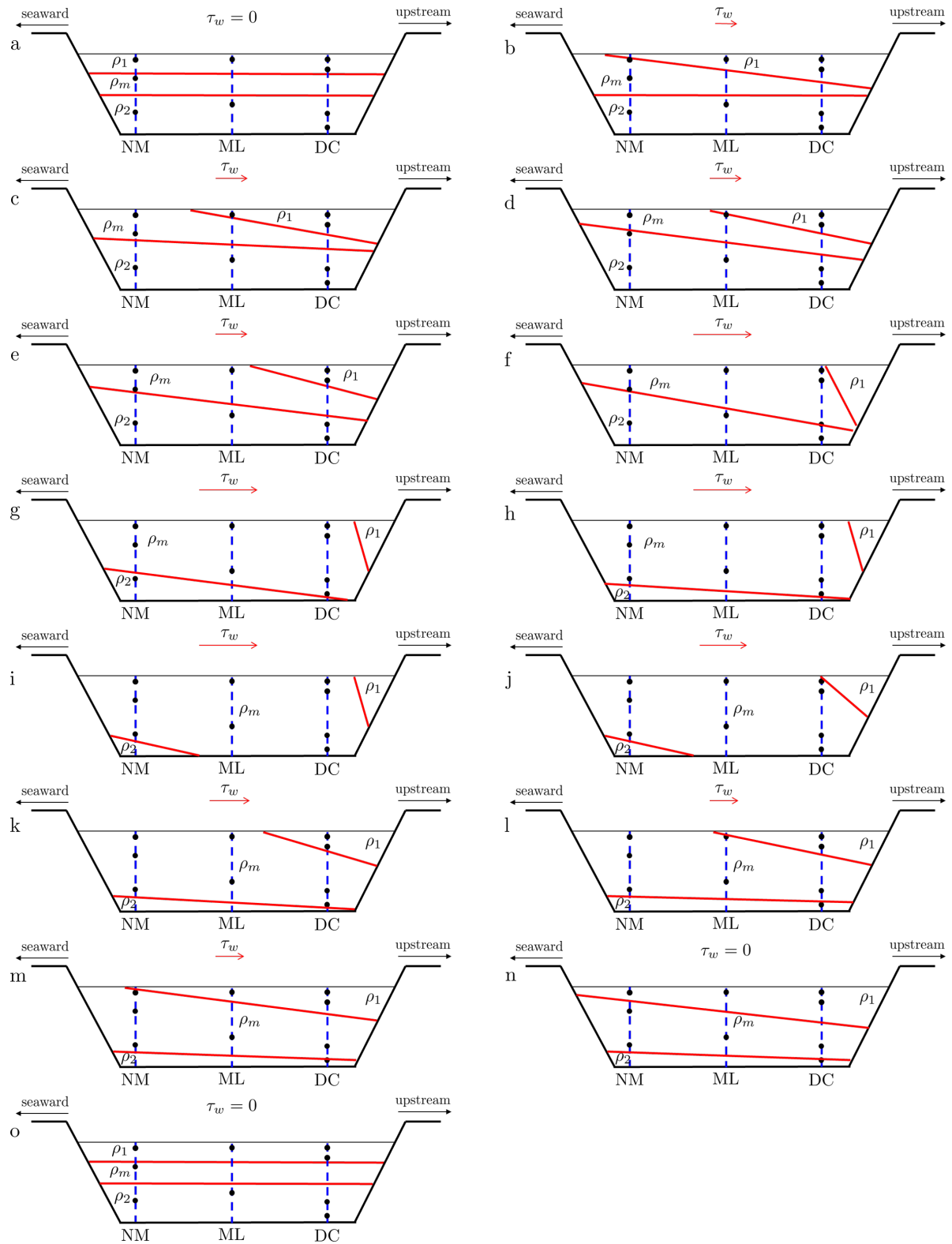


Figure 31: Movements of the density layers in Pescadero during the first wind event of the first period. The plots were constructed using the information given by the CTD.

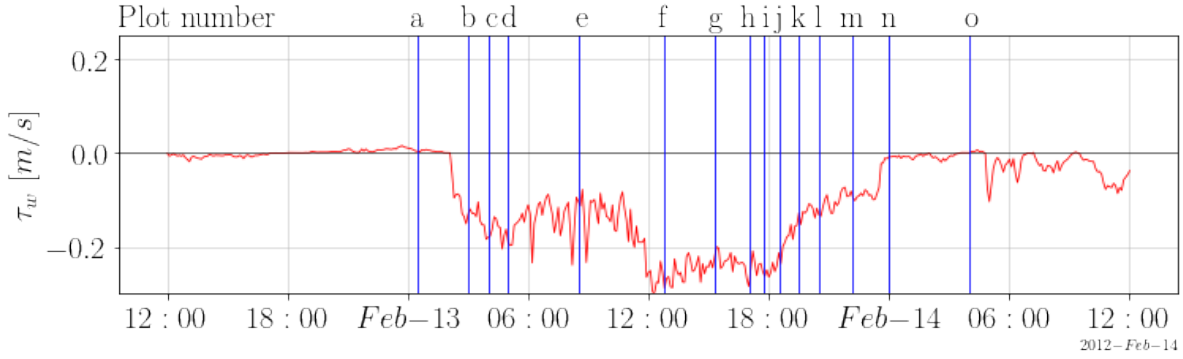


Figure 32: Wind event that was plotted in Fig. 31 with the instants of each plot.

After the second increase, we noticed a similar dynamic to after the first increase, but we didn't observe the flip happen. We observed that at the same time there was a wave overtopping event that probably affected the recirculation, but as it did not cause the same effect as before of negative velocities at the top its possible that it is not affecting the velocities with the same magnitude or it is overlapping the velocities of the relaxation changing its behavior. Another reason for the flip not happening is that the oscillation hadn't enough amplitude, so the seiche didn't happen.

Also, we studied the first wind event of the first period using the densities at locations NM, ML, and DC. In Fig. 31 we plotted the behavior of the layers according to the densities at different instants of time shown at Fig. 32. The sensors' positions were put in the horizontal center of the estuary and had a distance proportional to reality in the vertical for an easier estimation of the layers with the available information. During the wind event, the surface layer is moving landward due to the wind stress going in that direction, not being shown by any sensor at the biggest wind stress. The middle layer was occupying the water column for all the sensors during the peak of the wind event. The lower layer had an uncertain movement, but we drew it as the sensors were showing it, going in the same direction as the middle layer, not having the behavior of a third layer.

## 6.5 Freshwater input

The density time-series were showing a density decrease in time, especially at the bottom layer in NM and ML (Fig. 19), in DC we also observed a decrease but not in the deepest layer, in which we observed a light increase of density in the first period. The density decrease in time indicates a constant freshwater input. The parameter  $\Delta\rho/\Delta z$  is also slowly changing in time, a fact that is not observable in Fig. 23, but what is clear is the change between before and after a wind event that is decreasing over time, showing that wind stress is affecting each time less the estuarine structure. The last statement is also noticeable in the Wedderburn number (Fig. 22) where we observe in the last wind events W barely gets close to the threshold.

The destratification of the estuary could be a result of the freshwater constant input that is changing the density structure continuously in time. Also, it could be a result of the mixing that triggers the discharge increase during storm events, due to water's faster entrance to the estuary, which can induce interfacial instability (Katopodes, 2019). The discharge increase is only reflected in the estuary at the surface (Fig. 20) and is not very clear in the density, especially as it happens at the same time as a wind event in the first period and a wave overtopping event in the second period. It is possible that the rapid increase in the incoming flow

generate mixing, although there is not enough evidence to say that this is happening.

Like we said before, the two registered freshwater inflow increases happened with other events at the same time, the first one during a wind event and the other while there was wave overtopping. That is why we cannot attribute the changes observed in  $\hat{H}$ ,  $dh/dt$  or  $\Delta\hat{H}/\Delta x$  exclusively to discharge increase (Fig. 20). In Fig. 33 we observe discharge versus the water level and the level change over time. The first one had a strong correlation until  $Q$  started decreasing while  $H_{DC}$  still increase. The second plot also has some correlation, but we observe  $dh/dt$  is not increasing constant, so  $Q$  did not affect constantly the same at the water level increase rate, but still, there is a strong relationship between them.

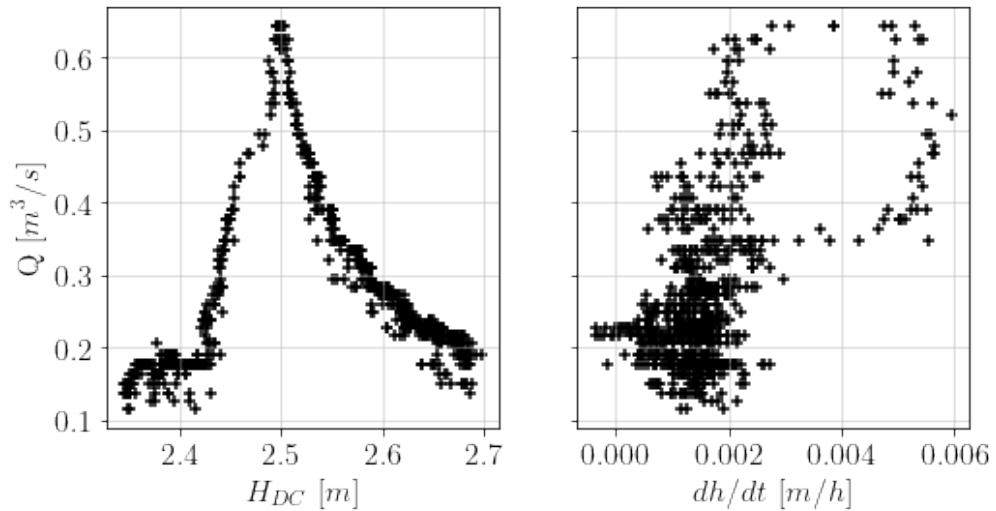


Figure 33: Discharge versus estuary height and discharge versus the height change in a 10-hour-frame for the period between 11 Feb. and 20 Feb..

Fig. 34 is showing the second discharge increase that happened at the same time as a wave overtopping event. We observed surface fluctuations in  $\hat{H}$  while it was increasing and  $\phi$  was increasing also, showing that Pescadero is stratifying instead of destratifying as was thought. When  $Q$  reached its highest value, it began to decrease and then became constant, while  $\phi$  kept increasing until the wind event when momentarily reached lower values. When the wind stopped  $\phi$  did not reach the same value that before showing the wind event reduced stratification.

The freshwater inflow is affecting stratification in the medium term and not in short term, not causing mixing when it increases, different from wind stress. Discharge is affecting the estuary by constantly and slowly reducing density.

## 6.6 Wave overtopping

Wave overtopping is an event that happens during high tide and relatively high significant wave height, but also can depend on the wave period or the wave direction. To determine the factors involved in this process Fig. 35 illustrates the tide level with significant wave height, dominant wave period, and dominant wave period direction as the estuary level rises. We noticed that two events happened with a significant wave height

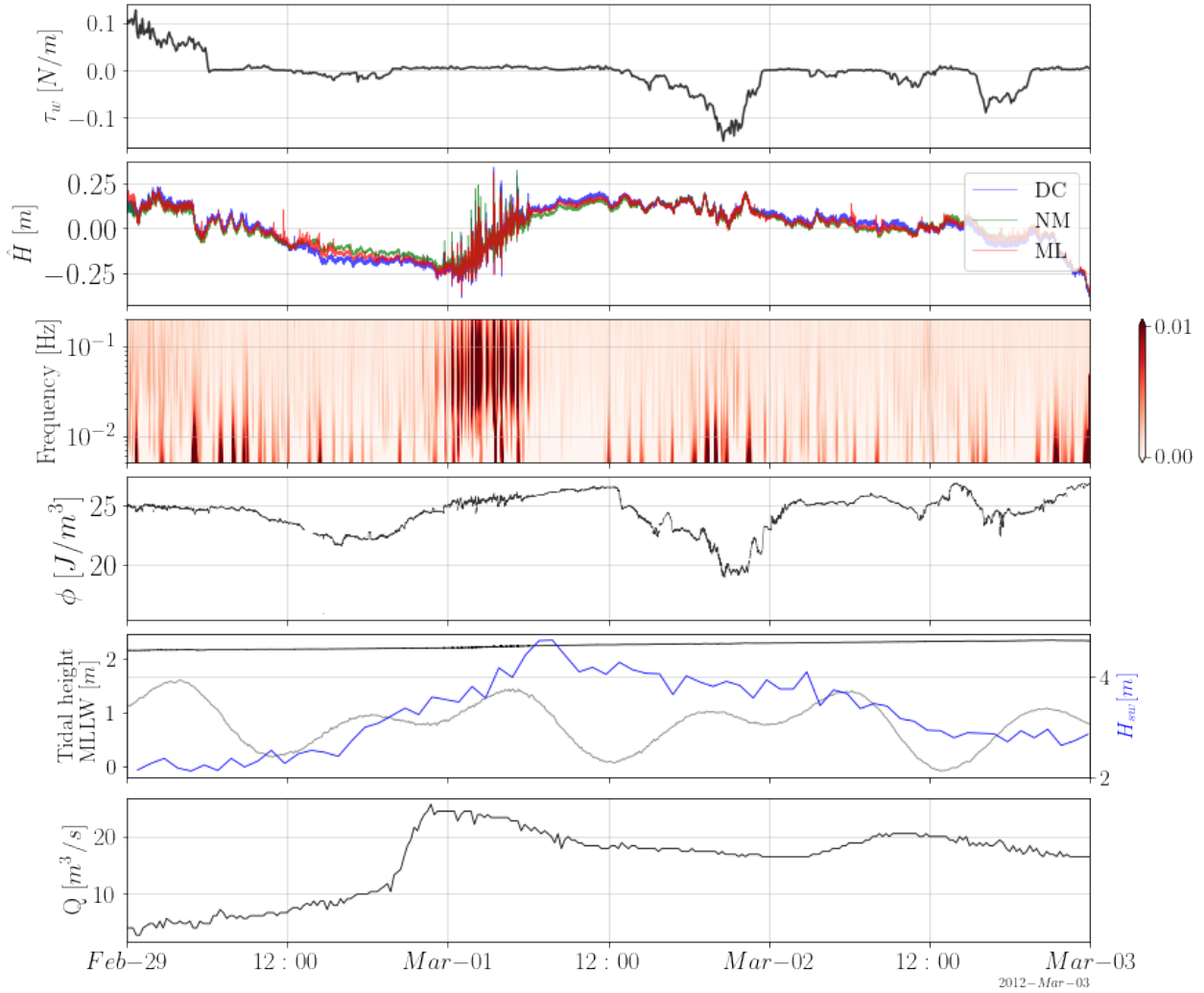


Figure 34: Time-series of wind stress ( $\tau_w$ ), standardized depth ( $\hat{H}$ ) in DC, NM, and ML locations, depth wavelet frequency analysis at DC, the potential energy anomaly ( $\phi$ ), significant wave height in Halfmoon Bay (blue), and tidal height in San Francisco (gray), and freshwater discharge ( $Q$ ).

between 4 and 6 m and the others between 2 and 4 m. For the dominant wave period, we didn't observe a clear pattern, but the direction of the dominant period showed the events occurred between  $300^\circ$  and  $325^\circ$ .

As we already mentioned wave overtopping causes changes in surface velocities, which led us to believe that there would be mixing in the estuary during these events due to the turbulent entry of the waves over the sand bar. However, we couldn't find any evidence of it causing destratification or decrease of the  $\phi$  in Fig. 34, probably because it wasn't an event big enough for the water level.

On the other hand, we observed a slow increase in density at the bottom layer of DC, which does not follow the same pattern of density decrease that the other locations had. In Fig. 36 there is a close-up of DC bottom density during the first period. First, we noticed that on 14 February there is an important wave overtopping event during which there is a negative spike in  $\rho_{DC}$ . After that, density started increasing but did not recover

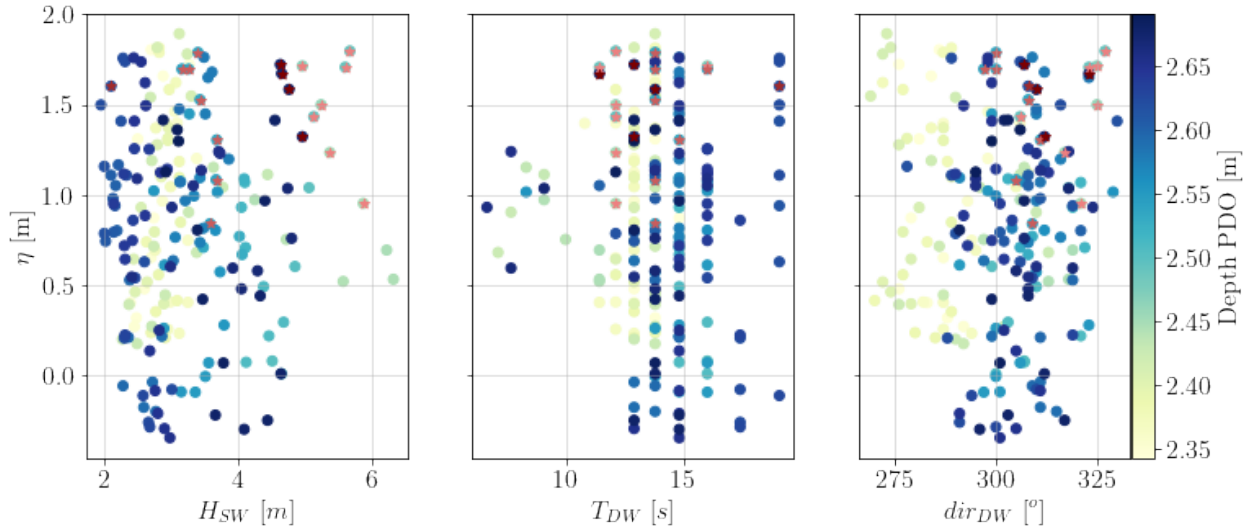


Figure 35: Tide level ( $\eta$ ) versus significant wave height ( $H_{SW}$ ), dominant wave period ( $T_{DW}$ ), and dominant wave period direction ( $dir_{DW}$ ) with the water level of Pescadero (Depth PDO) in colors, during the period between 11 Feb. and 20 Feb.. Four wave overtopping events were selected as the most prominent of the period and were marked in the plot with reddish stars.

its value from before the spike. This could mean there was mixing due to the action of the waves, but as at the same time, there was a  $Q$  increase we cannot attribute any driver in specific. It could be the action of both causing the spike.

After that, the wind would further reduce the density and, later, it would progressively increase. During that increase, we observed a smaller decrease during a wind event and another during a wave overtopping event on 17 February (Fig. 36). By observing this we can say that there is mixing due to the turbulent inflow of waves into the estuary that affects the deeper layer.

Also, the saline water inflow from the wave overtopping events could be causing the increase in density at the bottom of DC. The baroclinic effect could be making the saltwater set at the bottom slowly after the waves, but also it is possible that there is not enough saline water to change salinity and a baroclinic effect alone is acting in Pescadero.

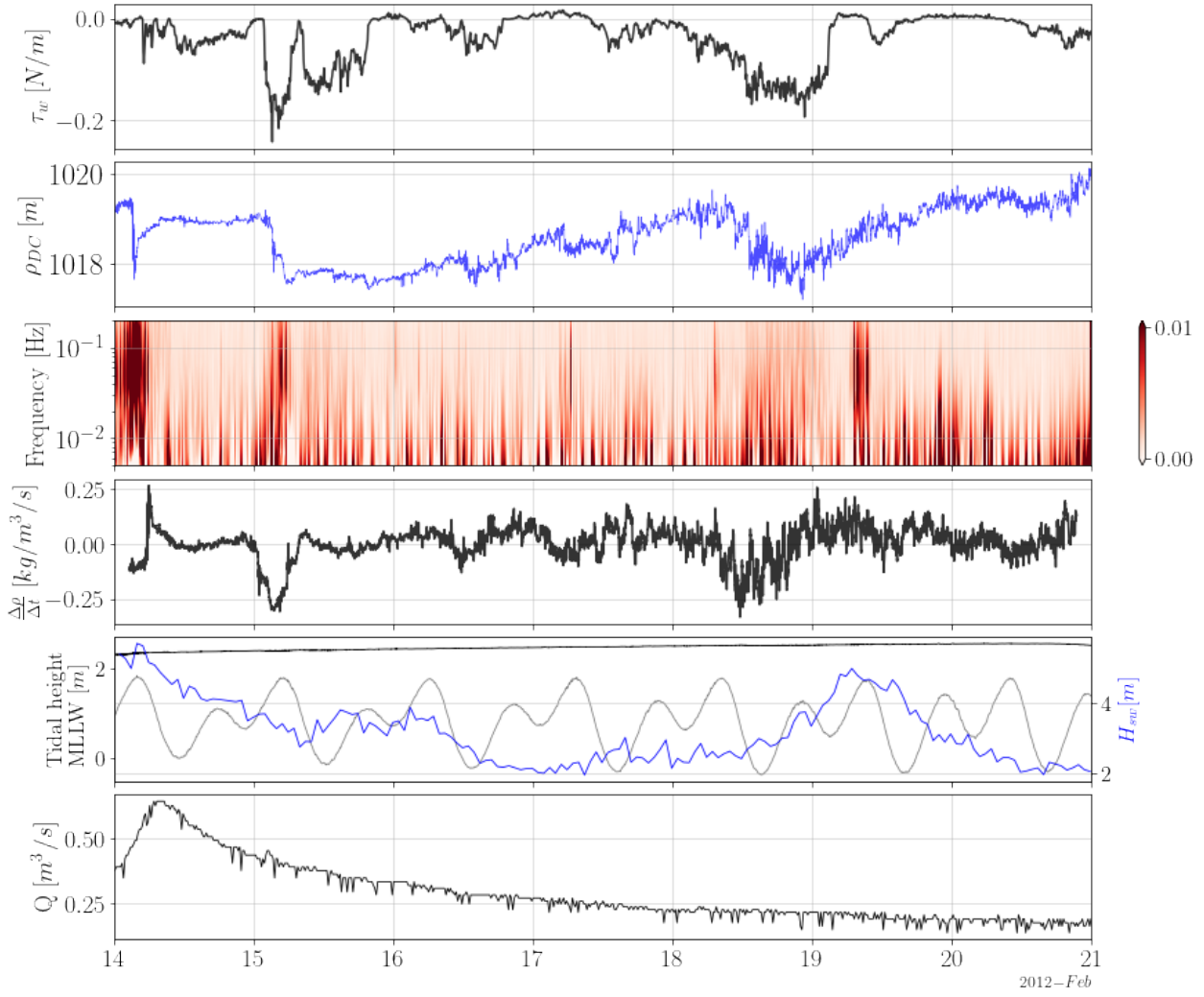


Figure 36: Time-series of wind stress ( $\tau_w$ ), bottom density in DC location ( $\rho_{DC}$ ), depth wavelet frequency analysis at DC, the change of density in a 10-hour time frame ( $\Delta\rho/\Delta t$ ), significant wave height in Halfmoon Bay (blue), tidal height in San Francisco (gray), and Pescadero estuary water level (black) in MLLW datum, and freshwater discharge ( $Q$ ).

## 7 Conclusion

The analyzes carried out showed how wind, freshwater inflow, and tide are influencing the stratification of the Pescadero estuary. We could notice that the constant discharge from Pescadero and Butano creek is changing water level and stratification in the estuary by increasing the epilimnion thickness. The latter, changes the lagoon response to wind forcing which was proved by buoyancy frequency behavior and potential energy anomaly. Consequently, the vertical exchange was reduced, limiting deep-water renewal. The latter could cause oxygen depletion which is associated with fish kills (Kelly et al., 2018).

We could observe that there was saltwater inflow caused by wave overtopping in the estuary, but it was not big enough to change stratification in long term. Anyways there was a slow increase in the deeper layer of DC location that could be driven by wave overtopping. We also observed some increases in the stratification

on the other layers but were only temporary and small. In addition, the wave overtopping did not cause an increase in water level either and only was visible as surface fluctuations. However, we noticed mixing during some wave overtopping events, depending on the water level, for higher levels we could not observe.

Wind force, on the other hand, caused a big impact in the estuarine dynamics, and was demonstrated to cause changes in density layers during and after wind influence (Fig. 25). It is shown that wind stress moved the layers causing upwelling during the wind events and, when stopped, stratified the water column but with different density changes between the surface and the bottom, demonstrating there was mixing present during the wind event.  $W$ ,  $\phi$ , and  $N^2$  demonstrate the effect of the wind in the watercolumn during the two study periods and how mixing is present (Figs. 21,22, 25). Upwelling magnitude is highly dependent on the duration of winds relative to the baroclinic setup time, including cases where wind duration is several times longer than the setup time (Roberts et al., 2021). The observed patterns during the wind events are consistent with the theory.

Pescadero Estuary is an ideal site for studying wind effects in the stratification due to the bi-directionality of wind caused by the estuarine morphology. That means that the study can be extrapolated easily to other bar-built estuaries. Also, for future studies, three-layer bi-dimensional models can be applied to account for all of the relevant processes, considering the high consistency between wind stress and the estuary.

In summary, wind stress significantly contributes to mixing the water column through upwelling in a small and highly stratified estuary. The density structure changes can result from a variety of processes. Which of these processes are relevant in a specific estuary depends on its morphology, its salinity, and also its stratification. The stratification and other conditions such as the area and depth at the estuary affect the occurrence of upwelling and mixing events. In the same way, changes in the wind stress events' magnitude and duration or in the estuarine morphologic conditions, including changes in water level, will have consequences for stratification and deep-water renewal mainly because of a change in upwelling occurrence. The results of this work could be applied to other small estuaries with seasonal or permanent closures like coastal lagoons.

## References

- Avalos Cueva, D., Monzón, C. O., Filonov, A., Tereshchenko, I., Limón Covarrubias, P., and Galaviz González, J. R. (2019). Natural frequencies of seiches in Lake Chapala. *Scientific Reports*, 9(1):1–11.
- Bastidas, L., Piedrahita, R., and Llanos-Rivera, A. (2021). A comparison of upwelling systems: A review of physical processes and ecosystem effects. *Progress in Oceanography*, 191:102475.
- Behrens, D. K., Bombardelli, F. A., and Largier, J. L. (2016). Landward propagation of saline waters following closure of a bar-built estuary: Russian River (California, USA). *Estuaries and Coasts*, 39(3):621–638.
- Behrens, D. K., Bombardelli, F. A., Largier, J. L., and Twohy, E. (2013). Episodic closure of the tidal inlet at the mouth of the Russian River—A small bar-built estuary in California. *Geomorphology*, 189:66–80.
- Clark, R. and O'Connor, K. (2019). A systematic survey of bar-built estuaries along the California coast. *Estuarine, Coastal and Shelf Science*, 226:106285.
- Coman, M. A. and Wells, M. G. (2012). Temperature variability in the nearshore benthic boundary layer of Lake Opeongo is due to wind-driven upwelling events. *Canadian Journal of Fisheries and Aquatic Sciences*, 69(2):282–296.

- Cousins, M., Stacey, M. T., and Drake, J. L. (2010). Effects of seasonal stratification on turbulent mixing in a hypereutrophic coastal lagoon. *Limnology and Oceanography*, 55(1):172–186.
- Curry, R., Houghton, R., Kidwell, T., and Tang, P. (1985). Pescadero marsh management: A plan for persistence and productivity.
- de la Fuente, A., Meruane, C., Contreras, M., Ulloa, H., and Niño, Y. (2010). Strong vertical mixing of deep water of a stratified reservoir during the Maule earthquake, central Chile (Mw 8.8). *Geophysical Research Letters*, 37(24).
- Dussaillant, A., Galdames, P., and Sun, C.-L. (2009). Water level fluctuations in a coastal lagoon: El yali ramsar wetland, chile. *Desalination*, 246(1-3):202–214.
- Gale, E., Pattiarchi, C., and Ranasinghe, R. (2006). Vertical mixing processes in intermittently closed and open lakes and lagoons, and the dissolved oxygen response. *Estuarine, Coastal and Shelf Science*, 69(1-2):205–216.
- Gupta, M., Williams, R. G., Lauderdale, J. M., Jahn, O., Hill, C., Dutkiewicz, S., and Follows, M. J. (2022). A nutrient relay sustains subtropical ocean productivity. *Proceedings of the National Academy of Sciences*, 119(41):e2206504119.
- Hewitt, J. E., Ellis, J. I., and Thrush, S. F. (2016). Multiple stressors, nonlinear effects and the implications of climate change impacts on marine coastal ecosystems. *Global change biology*, 22(8):2665–2675.
- Hoeksema, S. D., Chuwen, B. M., Tweedley, J. R., and Potter, I. C. (2018). Factors influencing marked variations in the frequency and timing of bar breaching and salinity and oxygen regimes among normally-closed estuaries. *Estuarine, Coastal and Shelf Science*, 208:205–218.
- Holt, J., Wakelin, S., Lowe, J., and Tinker, J. (2010). The potential impacts of climate change on the hydrography of the northwest european continental shelf. *Progress in Oceanography*, 86(3-4):361–379.
- Huber, E. R. and Carlson, S. M. (2020). Environmental correlates of fine-scale juvenile steelhead trout (*oncorhynchus mykiss*) habitat use and movement patterns in an intermittent estuary during drought. *Environmental Biology of Fishes*, 103(5):509–529.
- Human, L. R. D., Snow, G. C., and Adams, J. B. (2016). Responses in a temporarily open/closed estuary to natural and artificial mouth breaching. *South African Journal of Botany*, 107:39–48.
- Imam, Y. E., Laval, B., Pieters, R., and Lawrence, G. (2013). The strongly damped baroclinic response to wind in a multibasin reservoir. *Limnology and oceanography*, 58(4):1243–1258.
- Imberger, J. and Hamblin, P. F. (1982). Dynamics of lakes, reservoirs, and cooling ponds. *Annual Review of Fluid Mechanics*, 14(1):153–187.
- Jayaweera, H., Lowe, R., Zhang, H., and Pattiarchi, C. (2019). Turbulent mixing across the pycnocline under varying wind and buoyancy forcing: Observations from a coastal lagoon. *Journal of Geophysical Research: Oceans*, 124(8):6035–6054.
- Jones, P. D., New, M., Parker, D. E., Martin, S., and Rigor, I. G. (1999). Surface air temperature and its changes over the past 150 years. *Reviews of Geophysics*, 37(2):173–199.
- Katopodes, N. D. (2019). Chapter 11 - stratified flow. In Katopodes, N. D., editor, *Free-Surface Flow*, pages 780–839. Butterworth-Heinemann.

- Kelly, S., de Eyto, E., Dillane, M., Poole, R., Brett, G., and White, M. (2018). Hydrographic maintenance of deep anoxia in a tidally influenced saline lagoon. *Marine and Freshwater Research*, 69(3):432–445.
- Kundu, P. K., Cohen, I. M., and Dowling, D. R. (2015). *Fluid Mechanics*. Academic press.
- Large, W. and Pond, S. (1981). Open ocean momentum flux measurements in moderate to strong winds. *Journal of Physical Oceanography*, 11(3):324–336.
- Largier, J. (2021). Hydrological responses to closure in Californian estuaries. Coastal & Marine Sciences Institute, University of California Davis, Global Forum on Intermittent Estuaries. <https://www.youtube.com/watch?v=HXWZNu1KYMQ&t=140s>.
- Largier, J., Aiello, I., Jacobs, D., Lacy, J., Pallud, C., Stacey, M., Carlson, S., Huber, E., and Bowles, C. (2015). Report of pescadero lagoon science panel. [https://repository.library.noaa.gov/view/noaa/40845/noaa\\_40845\\_DS1.pdf](https://repository.library.noaa.gov/view/noaa/40845/noaa_40845_DS1.pdf).
- Laudier, N. A., Thornton, E. B., and MacMahan, J. (2011). Measured and modeled wave overtopping on a natural beach. *Coastal Engineering*, 58(9):815–825.
- Laval, B. E., Morrison, J., Potts, D. J., Carmack, E. C., Vagle, S., James, C., McLaughlin, F. A., and Foreman, M. (2008). Wind-driven summertime upwelling in a fjord-type lake and its impact on downstream river conditions: Quesnel Lake and River, British Columbia, Canada. *Journal of Great Lakes Research*, 34(1):189–203.
- Lee, G., Gommers, R., Waselewski, F., Wohlfahrt, K., and O’Leary, A. (2019). Pywavelets: A python package for wavelet analysis. *Journal of Open Source Software*, 4(36):1237.
- MacIntyre, S., Rueda, F. J., and S’anchez-Garc’ia, E. (2010). Ecosystem responses to coastal upwelling: A comparison of four major eastern boundary upwelling systems. *Journal of Marine Systems*, 83(3-4):244–255.
- Marti-Cardona, B., Steissberg, T., Schladow, S. G., and Hook, S. (2008). Relating fish kills to upwellings and wind patterns in the salton sea. In *The Salton Sea Centennial Symposium*, pages 85–95. Springer.
- Martínez, M. L., Intralawan, A., Vázquez, G., Pérez-Maqueo, O., Sutton, P., and Landgrave, R. (2007). The coasts of our world: Ecological, economic and social importance. *Ecological Economics*, 63(2-3):254–272.
- McSweeney, S., Kennedy, D., Rutherford, I., and Stout, J. (2017). Intermittently closed/open lakes and lagoons: Their global distribution and boundary conditions. *Geomorphology*, 292:142–152.
- Monismith, S. G. (1985). Wind-forced motions in stratified lakes and their effect on mixed-layer shear. *Limnology and oceanography*, 30(4):771–783.
- Monismith, S. G., Kimmerer, W. J., and Burau, J. R. (2006). Vertical mixing and coastal upwelling in stratified, tidally mixed estuaries. *Estuaries and Coasts*, 29(2):347–361.
- Neumann, B., Vafeidis, A. T., Zimmermann, J., and Nicholls, R. J. (2015). Future coastal population growth and exposure to sea-level rise and coastal flooding-a global assessment. *PloS one*, 10(3):e0118571.
- Nidheesh, A., Gandhimathi, R., and Suguna, J. (2018). Stratification dynamics in a freshwater reservoir under changing thermal regime. *Journal of Hydro-environment Research*, 19:9–19.

- Nunes, M. and Adams, J. (2014). Responses of primary producers to mouth closure in the temporarily open/closed Great Brak Estuary in the warm-temperate region of South Africa. *African Journal of Aquatic Science*, 39(4):387–394.
- Omstedt, A., Pettersen, C., Rodhe, J., and Winsor, P. (2004). Baltic Sea climate: 200 yr of data on air temperature, sea level variation, ice cover, and atmospheric circulation. *Climate Research*, 25(3):205–216.
- Paugam, C., Sous, D., Rey, V., Meulé, S., Faure, V., Boutron, O., Luna-Laurent, E., and Migne, E. (2021). Wind tides and surface friction coefficient in semi-enclosed shallow lagoons. *Estuarine, Coastal and Shelf Science*, 257:107406.
- Peeters, F. and Kipfer, R. (2009). Currents in stratified water bodies 1: Density-driven flows. In Likens, G. E., editor, *Encyclopedia of Inland Waters*, pages 530–538. Academic Press, Oxford.
- Ranasinghe, R. and Pattiaratchi, C. (1999). The seasonal closure of tidal inlets: Wilson Inlet—a case study. *Coastal Engineering*, 37(1):37–56.
- Ranasinghe, R. and Pattiaratchi, C. (2003). The seasonal closure of tidal inlets: causes and effects. *Coastal engineering journal*, 45(04):601–627.
- Read, J. S., Hamilton, D. P., Jones, I. D., Muraoka, K., Winslow, L. A., Kroiss, R., Wu, C. H., and Gaiser, E. (2011). Derivation of lake mixing and stratification indices from high-resolution lake buoy data. *Environmental Modelling & Software*, 26(11):1325–1336.
- Richards, C. M., Moal, O., and Pallud, C. (2018). Changes in water quality following opening and closure of a bar-built estuary (pescadero, California). *Marine Chemistry*, 198:10–27.
- Roberts, D. C., Egan, G. C., Forrest, A. L., Largier, J. L., Bombardelli, F. A., Laval, B. E., Monismith, S. G., and Schladow, G. (2021). The setup and relaxation of spring upwelling in a deep, rotationally influenced lake. *Limnology and Oceanography*, 66(4):1168–1189.
- Schernewski, G. (2002). *Baltic Coastal Ecosystems: Structure, Function and Coastal Zone Management*. Springer Science & Business Media.
- Schmidtko, S., Stramma, L., and Visbeck, M. (2017). Decline in global oceanic oxygen content during the past five decades. *Nature*, 542(7641):335–339.
- Shintani, T., de la Fuente, A., de la Fuente, A., Niño, Y., and Imberger, J. (2010). Generalizations of the Wedderburn number: Parameterizing upwelling in stratified lakes. *Limnology and Oceanography*, 55(3):1377–1389.
- Simpson, J. and Hunter, J. (1974). Fronts in large lakes: An example from lake malawi. *Limnology and Oceanography*, 19(2):202–204.
- Simpson, J. H., Brown, J., Matthews, J., and Allen, G. (1985). Tidal straining, density currents, and stirring in the control of estuarine stratification. *Estuaries*, 13:125–132.
- Sloan, R. M. (2006). Ecological investigations of a fish kill in Pescadero Lagoon, California. 3032. Master's Theses.
- Stevens, C. and Imberger, J. (1996). The initial response of a stratified lake to a surface shear stress. *Journal of Fluid Mechanics*, 312:39–66.

- Teledyne, R. I. (2008). Adcp coordinate transformation: Formulas and calculations.
- Thorne, K. M., Buffington, K. J., Jones, S. F., and Largier, J. L. (2021). Wetlands in intermittently closed estuaries can build elevations to keep pace with sea-level rise. *Estuarine, Coastal and Shelf Science*, 257:107386.
- Valerio, G., Pilotti, M., Marti, C. L., and rg Imberger, J. (2012). The structure of basin-scale internal waves in a stratified lake in response to lake bathymetry and wind spatial and temporal distribution: Lake Iseo, Italy. *Limnology and Oceanography*, 57(3):772–786.
- Viaroli, P., Bartoli, M., Giordani, G., Naldi, M., Orfanidis, S., and Zaldivar, J. M. (2008). Community shifts, alternative stable states, biogeochemical controls and feedbacks in eutrophic coastal lagoons: a brief overview. *Aquatic Conservation: Marine and Freshwater Ecosystems*, 18(S1):S105–S117.
- Welch, P. (1967). The use of fast Fourier transform for the estimation of power spectra: a method based on time averaging over short, modified periodograms. *IEEE Transactions on audio and electroacoustics*, 15(2):70–73.
- Whitfield, A. and Bate, G. (2007). A review of information on temporarily open/closed estuaries in the warm and cool temperate biogeographic regions of South Africa, with particular emphasis on the influence of river flow on these systems. *Water Research Commission, Report*, 1581(1):07.
- Whitfield, A. and Wooldridge, T. (1994). Changes in freshwater supplies to southern african estuaries: some theoretical and practical considerations. *OLSEN & OLSEN, FREDENSBORG, DENMARK.*, pages 41–50.
- Williams, J. et al. (1990). Pescadero marsh natural preserve hydrologic enhancement plan. *Prepared for California Department of Parks and Recreation. Report no. 504, 31 August. Prepared by Phillip Williams and Associates, San Francisco, California.*
- Williams, M. (2014). Hydrodynamics and salt dispersion in intermittently closed bar-built estuaries. *PhD Thesis*. UC Berkeley.
- Williams, M. and Stacey, M. T. (2016). Tidally discontinuous ocean forcing in bar-built estuaries: The interaction of tides, infragravity motions, and frictional control. *Journal of Geophysical Research: Oceans*, 121(1):571–585.
- Winckler, P., Aguirre, C., Farías, L., Contreras-López, M., and Masotti, I. (2020). Evidence of climate-driven changes on atmospheric, hydrological, and oceanographic variables along the chilean coastal zone. *Climatic Change*, 163(2):633–652.
- Winckler Grez, P., Aguirre, C., Farías, L., Contreras-López, M., and Masotti, I. (2020). Evidence of climate-driven changes on atmospheric, hydrological, and oceanographic variables along the chilean coastal zone. *Climatic Change*, 163(2):633–652.
- Woolway, R. I., Meinson, P., Nôges, P., Jones, I. D., and Laas, A. (2017). Atmospheric stilling leads to prolonged thermal stratification in a large shallow polymictic lake. *Climatic Change*, 141(4):759–773.
- Xu, D., Hesser, T., and Mayer, T. (2017). Vertical exchange and interfacial layer dynamics in two-layered shallow estuaries. *Journal of Geophysical Research: Oceans*, 122(7):5506–5525.